Electronic Supplementary Material (ESI) for Inorganic Chemistry Frontiers.

Supporting Information for

Conjugated Schiff-base macrocycle weakens the transverse crystal field of air-stable dysprosium single-molecule magnets

Shuting Liu,[a, b] Yolimar Gil,[d] Chen Zhao,[a, b] Jinjiang Wu,[a, b] Zhenhua Zhu,[a] Xiao-Lei Li,[a] Daniel Aravena,*[c] and Jinkui Tang*[a, b]

[a] State Key Laboratory of Rare Earth Resource Utilization, Changchun Institute of Applied Chemistry, Chinese Academy of Sciences, Changchun 130022, P. R. China.
[b] School of Applied Chemistry and Engineering, University of Science and Technology of China, Hefei 230026, P. R. China.
[c] Departamento de Química de los Materiales, Facultad de Química y Biología, Universidad de Santiago de Chile, Casilla 40, Correo 33, Santiago, Chile.
[d] Facultad de Ciencias Químicas y Farmacéuticas, Universidad de Chile, Casilla 233, Santiago, Chile.

Table of contents

I. General procedures 2

II. Synthesis and characterization 3

III. X-ray crystallography 8

IV. Magnetic characterization 26

V. Computational details 50

VI. References 56

I. General procedures

Unless stated otherwise, all solvents and chemicals were used as received. Coordination reactions were carried out under aerobic conditions. **Elemental analyses** (C, H, and N) were performed by PerkinElmer 2400 analyzer. **Fourier Transform infrared spectrum** (FT-IR) was recorded on a Nicolet 6700 Flex FTIR spectrometer equipped with a smart iTR attenuated total reflectance (ATR) sampling accessory and labeled according to their relative intensities with vs (very strong), s (strong), m (medium), and w (weak). **Circular dichroism** (CD) spectra data were collected on a Jasco J-820 spectropolarimeter at room temperature. **Powder X-ray diffraction** (PXRD) data were collected on a Bruker D8 advance X-ray diffractometer using Cu Kα radiation (λ = 1.54184 Å) over the range of 5-50°. **Thermogravimetric analyses** (TGA) were performed on a Netzsch STA 449F3 analyzer under N_2 atmosphere from room temperature to 800 °C at a heating rate of 10 °C/min. **Single-crystal X-ray diffraction** (SCXRD) measurements were collected on a Bruker D8 Venture CCD diffractometer with graphite-monochromated Mo Kα radiation (λ = 0.71073 Å). The crystal was collected at 180 K. The program APEX3 was used to integrate the data, which were thereafter corrected for absorption using multi-scan method. The structures were solved by intrinsic phasing methods and refined by full-matrix least-squares methods on F^2 with anisotropic thermal parameters for all non-hydrogen atoms by using the SHELXT[1] (intrinsic phasing methods) and refined by SHELXL[2] (full matrix least-squares techniques) in the Olex2[3] package. All non-hydrogen atoms were refined with anisotropic displacement parameters. The hydrogen atoms were introduced in calculated positions and refined with a fixed geometry with respect to their carrier atoms. Crystallographic data, refinement details and CCDC number are given in Table S1-S3. **Magnetic susceptibility measurements** were performed using a Quantum Design MPMS-XL7 SQUID magnetometer. Variable-temperature direct current (dc) magnetic susceptibility were collected with an external magnetic field of 1000 Oe in the temperature range of 2-300 K and variable field magnetization data from ±7 T were collected. Alternating current (ac) magnetic susceptibility data were collected in zero applied field using a 3.0 Oe ac oscillating field. The experimental magnetic data were corrected for the diamagnetism estimated from Pascal's constants[4] and sample holder calibration.

II. Synthesis and characterization

8-aminoquinoline-2-carbaldehyde was prepared via a previously published method.[5, 6] Potassium (3-bromophenyl)triphenylborate and potassium (4-bromophenyl)triphenylborates were synthesized according literature procedures.[7]

Synthetic strategy for **1**: 8-aminoquinoline-2-carbaldehyde (0.0517 g, 0.3 mmol) was added to acetonitrile (15 mL) together with $Dy(ClO_4)_3 \cdot 6H_2O$ (0.0569 g, 0.1 mmol). The reaction was kept at 80 ℃ for 24 h. Centrifugation was used to remove the precipitate from the solution. Ph_3SiOH (0.0553 g, 0.2 mmol) and Et_3N (28 μL, 0.2 mmol) were added to supernatant. The reaction was kept at 80 ℃ for another 12 h. After cooling to room temperature, the mixture was filtered to give a clear dark orange solution. Orange block crystals suitable for single crystal diffraction were obtained after slow evaporation of solvent for one week (yield: 21 mg, 16%, based on dysprosium). Elemental analysis calculated for $C_{66}H_{50}ClDyN_6O_7Si_2$ (%): C, 61.30; H, 3.90; N, 6.50. Found (%): C, 61.63; H, 3.58; N, 6.56. Selected IR (cm^{-1}): 621 (s), 700 (vs), 741 (m), 799 (w), 842 (w), 853 (w), 944 (s), 1088 (s), 1142 (w), 1223 (m), 1270 (w), 1315 (w), 1375 (w), 1426 (m), 1470 (w), 1511 (m), 1557 (w), 1588 (w), 1609 (w), 1971 (w), 3024 (br).

Synthetic strategy for **2**: Using the procedure described above for **1**, $Dy(OTf)_3 \cdot 9H_2O$ (0.0772 g, 0.1 mmol) was used to give **2** as orange block crystals (yield: 26 mg, 19%, based on dysprosium). Elemental analysis calculated for $C_{67}H_{48}DyF_3N_6O_5SSi_2$ (%): C, 60.74; H, 3.65; N, 6.34. Found (%): C, 60.39; H, 3.41; N, 6.31. Selected IR (cm^{-1}): 571 (w), 634 (s), 699 (vs), 741 (m), 765 (w), 798 (w), 850 (m), 889 (w), 942 (s), 997 (w), 1028 (s), 1105 (m), 1147 (m), 1222 (m), 1255 (s), 1319 (m), 1377 (w), 1426 (m), 1470 (w), 1512 (m), 1558 (w), 1587 (w), 1608 (w), 1959 (w), 3064 (br).

Synthetic strategy for **3R**: (1R,2R)-cyclohexane-1,2-diamine (0.0228 g, 0.2 mmol) and pyridine-2,6-dicarbaldehyde (0.0270 g, 0.2 mmol) were dissolved to methanol (20 mL), followed by addition of $DyCl_3 \cdot 6H_2O$ (0.0377 g, 0.1 mmol). The mixture was refluxed for 12 h and methanol was evaporated under reduced pressure, yielding an orange powder. The orange solid was dissolved in a mixture solvent of 20 mL DCM and 20 mL H_2O. Ph_3SiOH (0.0553 g, 0.2 mmol), Et_3N (28 μL, 0.2 mmol) and potassium (3-bromophenyl)triphenylborates (0.0437 g, 0.1 mmol) were added to the above mentioned mixture in turn. The mixture was heated at 70 ℃ for 1 h, then cooling to room temperature. The DCM phase was separated and filtered, giving a yellow clear solution. The light-yellow block crystals suitable for X-ray diffraction were obtained by layering the DCM phase with n-pentane at room temperature for 4 days (yield: 50 mg, 29%, based on dysprosium). Elemental analysis calculated for $C_{86}H_{81}BBrDyN_6O_3Si_2$ (%): C, 66.38; H, 5.25; N 5.40. Found (%): C, 66.46; H, 4.79; N 5.45. Selected IR (cm^{-1}): 561(m), 574(m), 611(s), 655(s), 697(vs), 737(s), 773(w), 857(m), 957(vs), 1000(m), 1008(m), 1030(m), 1045(m), 1103(s), 1163(m), 1273(m), 1384(w), 1426(s),1448(w) 1462(m), 1592(m), 1650(w), 2857(w), 2932(w), 3057(w).

Synthetic strategy for **3S**: Using the procedure described above for **3R**, (1S,2S)-cyclohexane-1,2-diamine (0.0228 g, 0.2 mmol) was used to give **3S** as light-yellow crystals (yield: 47 mg, 29%, based on dysprosium) Elemental analysis calculated for $C_{86}H_{81}BBrDyN_6O_3Si_2$ (%): C, 66.38; H, 5.25; N 5.40. Found (%): C, 66.16; H, 4.78; N 5.43. Selected IR (cm^{-1}): 559(w), 579(m), 611(s), 666(m), 700(vs), 736(s), 800(m), 861(m), 969(vs), 1000(m), 1007(m), 1031(m), 1105(s), 1164(w), 1426(s),

1477(m), 1591(s), 1649(m), 2859(w), 2931(w), 3057(w).

Synthetic strategy for **4R**: Using the procedure described above for **3R**, potassium (4-bromophenyl)triphenylborates (0.0437 g, 0.1 mmol) was used to give **4R** as light-yellow crystals (yield: 50 mg, 29%, based on dysprosium). Elemental analysis calculated for $C_{86}H_{81}BBrDyN_6O_3Si_2$ (%): C, 66.38; H, 5.25; N 5.40. Found (%): C, 65.81; H, 4.76; N 5.32. Selected IR (cm^{-1}): 561(m), 574(m), 611(s), 655(s), 697(vs), 737(s), 773(w), 857(m), 957(vs), 1000(m), 1008(m), 1030(m), 1045(m), 1103(s), 1163(m), 1273(m), 1384(w), 1426(s),1448(w) 1462(m), 1592(m), 1650(w), 2857(w), 2932(w), 3057(w).

Synthetic strategy for **4S**: Using the procedure described above for **3R**, (1S,2S)-cyclohexane-1,2-diamine (0.0228 g, 0.2 mmol) and potassium (4-bromophenyl)triphenylborates (0.0437 g, 0.1 mmol) were combined to give **4S** as light-yellow crystals (yield: 40 mg, 23%, based on dysprosium). Elemental analysis calculated for $C_{86}H_{81}BBrDyN_6O_3Si_2$ (%): C, 66.38; H, 5.25; N 5.40. Found (%): C, 66.55; H, 4.82; N 5.41. Selected IR (cm^{-1}): 561(m), 579(m), 611(s), 655(s), 697(vs), 739(s), 774(w), 860(m), 957(vs), 1000(m), 1008(m), 1030(m), 1045(m), 1103(s), 1163(m), 1273(m), 1384(w), 1426(s),1448(w) 1462(m), 1592(m), 1650(w),2845(w), 2932(w), 3057(w).

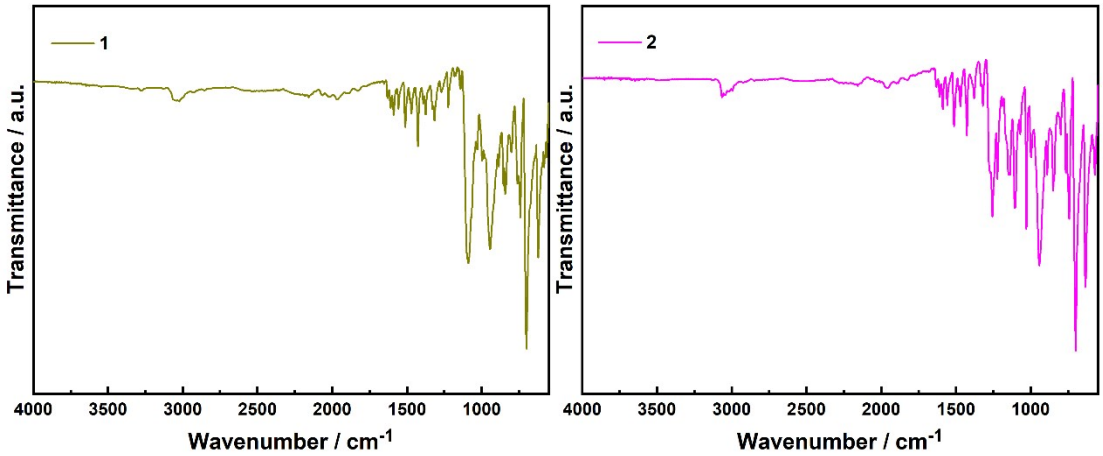

Figure S1. IR spectra of **1** and **2**.

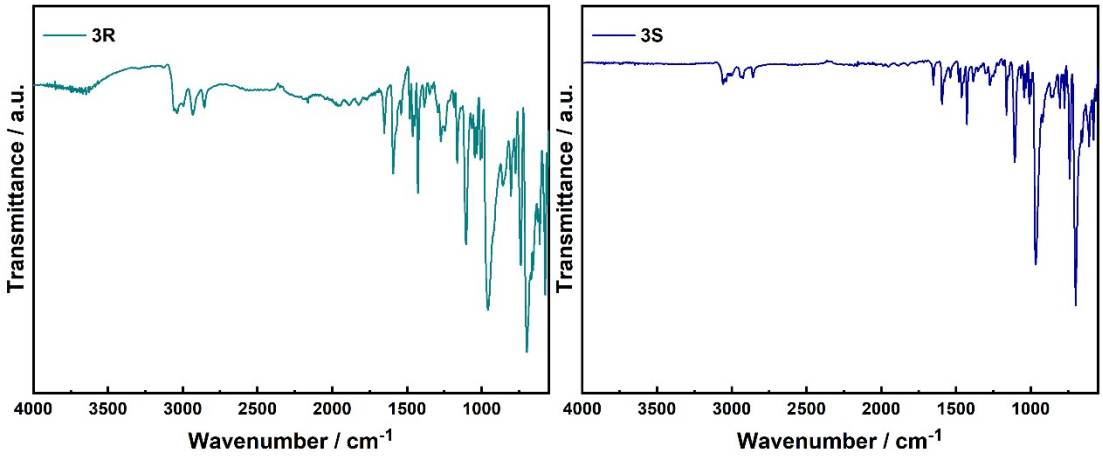

Figure S2. IR spectra of **3R** and **3S**.

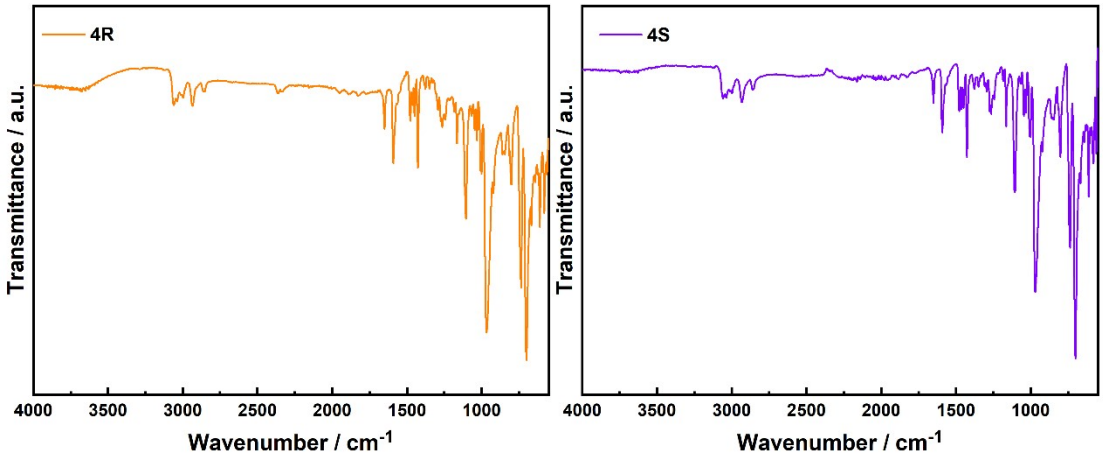

Figure S3. IR spectra of **4R** and **4S**.

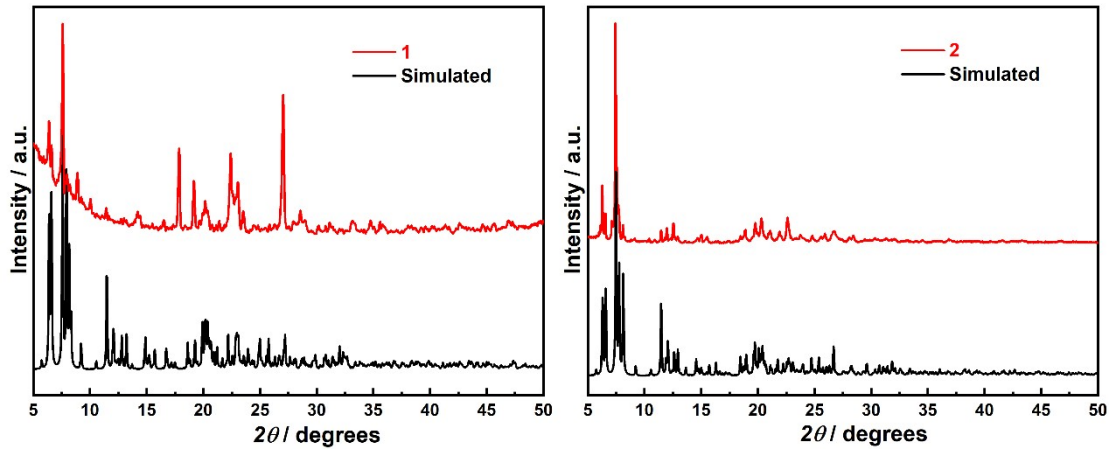

Figure S4. Experimental (red) and simulated (black) PXRD patterns for **1** and **2** in the range of 5-50°.

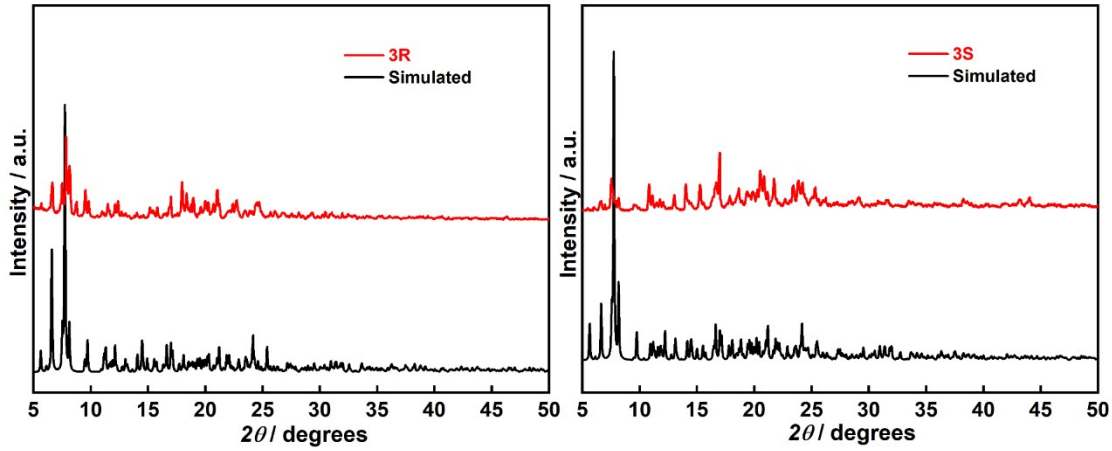

Figure S5. Experimental (red) and simulated (black) PXRD patterns for **3R** and **3S** in the range of 5-50°.

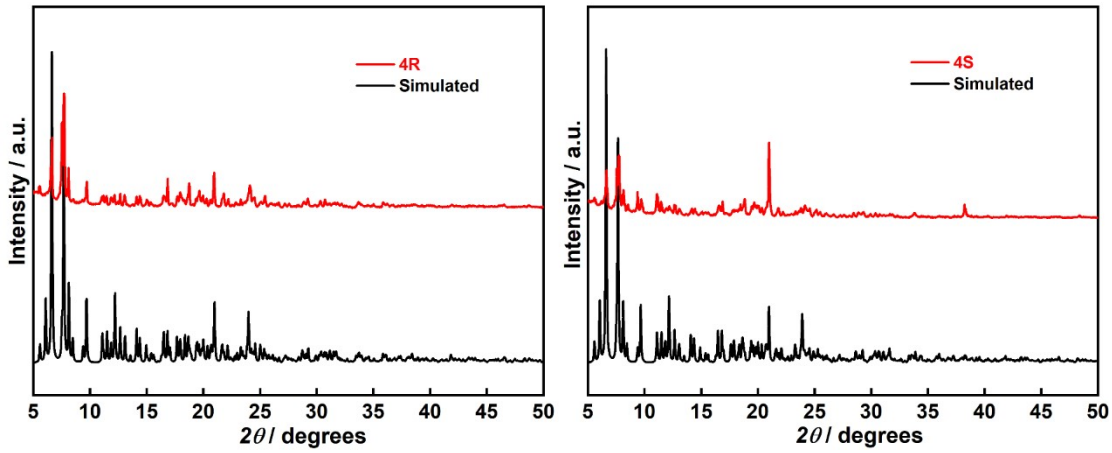

Figure S6. Experimental (red) and simulated (black) PXRD patterns for **4R** and **4S** in the range of 5-50°.

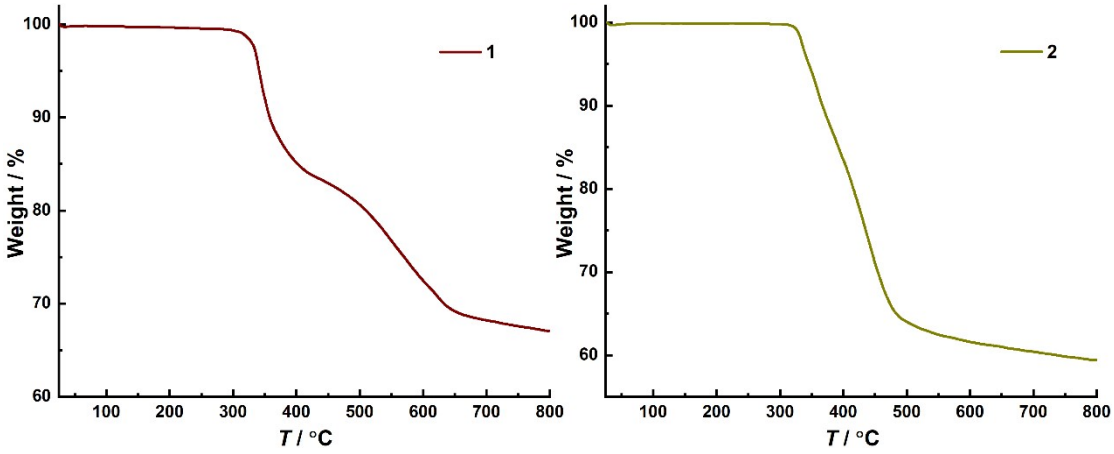

Figure S7. Thermogravimetric analysis for **1** and **2** under N_2 atmosphere.

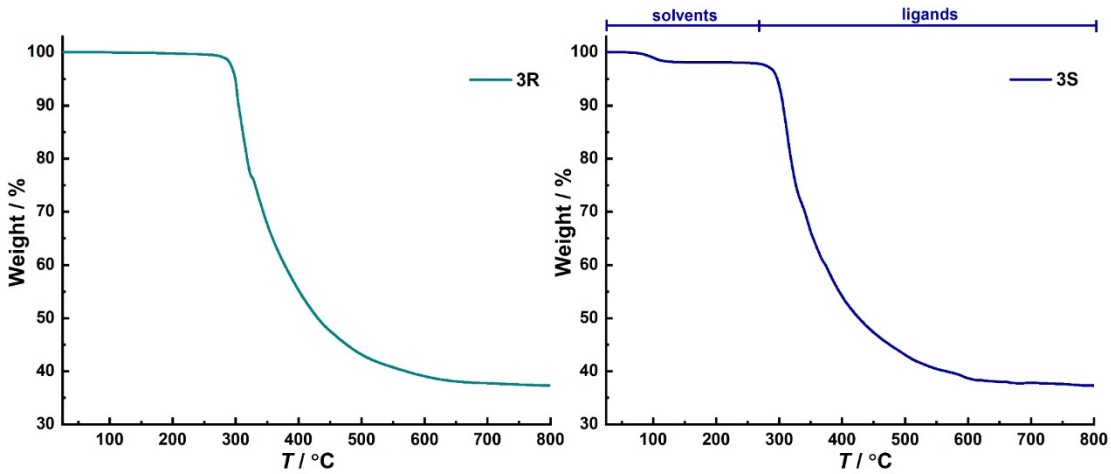

Figure S8. Thermogravimetric analysis for **3R** and **3S** under N_2 atmosphere.

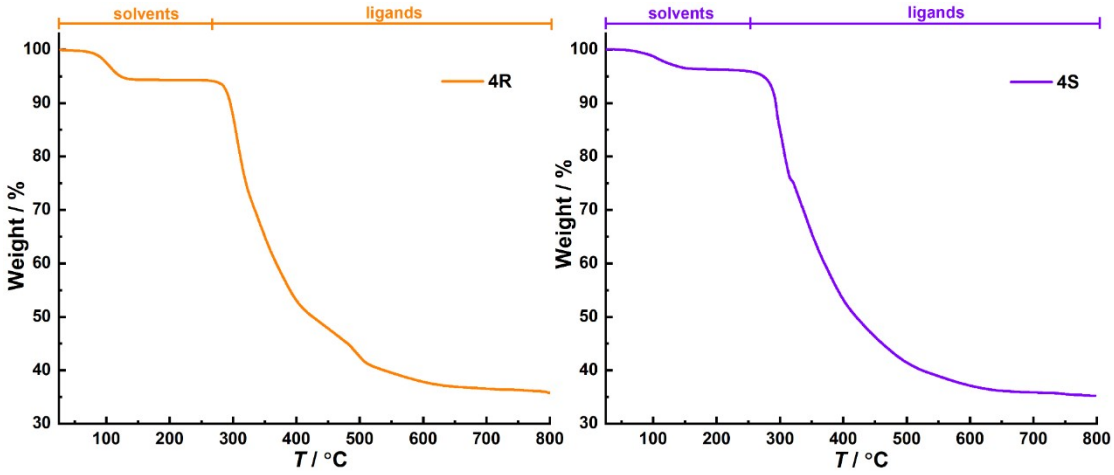

Figure S9. Thermogravimetric analysis for **4R** and **4S** under N_2 atmosphere.

III. X-ray crystallography

Table S1. Crystallographic data of the precursor complexes **A** and **B**.

Identification code	**A**	**B**
Empirical formula	$C_{32}H_{27}Cl_3DyN_7O_{15}$	$C_{26}H_{30}Cl_3DyN_6$
Formula weight	1018.45	695.41
Temperature/K	180.0	180.0
Crystal system	orthorhombic	monoclinic
Space group	*P*bca	*C*2/c
a/Å	17.2493(4)	16.9787(7)
b/Å	20.2699(5)	17.1471(7)
c/Å	21.2300(4)	12.8817(5)
α/°	90	90
β/°	90	122.593(2)
γ/°	90	90
Volume/Å^3	7422.9(3)	3159.7(2)
Z	8	4
ρ_{calc}g/cm^3	1.823	1.462
μ/mm^{-1}	2.311	2.642
F(000)	4040.0	1380.0
Crystal size/mm^3	0.15 × 0.12 × 0.1	0.23 × 0.2 × 0.1
Radiation	MoKα (λ = 0.71073)	MoKα (λ = 0.71073)
2Θ range for data collection/°	4.454 to 52.092	6.538 to 50.106
Index ranges	-21 ≤ h ≤ 19, -25 ≤ k ≤ 25, -23 ≤ l ≤ 26	-20 ≤ h ≤ 20, -20 ≤ k ≤ 20, -15 ≤ l ≤ 13
Reflections collected	53064	14376
Independent reflections	7278 [R_{int} = 0.0314, R_{sigma} = 0.0183]	2781 [R_{int} = 0.0241, R_{sigma} = 0.0176]
Data/restraints/parameters	7278/1373/781	2781/0/164
Goodness-of-fit on F^2	1.045	1.109
Final R indexes [I>=2σ (I)]	R_1 = 0.0669, wR_2 = 0.1898	R_1 = 0.0221, wR_2 = 0.0556
Final R indexes [all data]	R_1 = 0.0753, wR_2 = 0.1992	R_1 = 0.0244, wR_2 = 0.0580
Largest diff. peak/hole / e Å^{-3}	2.22/-1.67	0.56/-1.04
CCDC number	2178776	2178777

Table S2. Crystallographic data of complex **1**, **2** and **3R**.

Identification code	**1**	**2**	**3R**
Empirical formula	$C_{68}H_{51}ClDyN_7O_6Si_2$	$C_{69}H_{51}DyF_3N_7O_5SSi_2$	$C_{88}H_{85}BBrCl_4DyN_6O_3Si_2$
Formula weight	1316.28	1365.91	1725.82
Temperature/K	180.0	180.0	180.0
Crystal system	triclinic	triclinic	orthorhombic
Space group	$P\bar{1}$	$P\bar{1}$	$P2_12_12_1$
a/Å	14.3908(4)	14.5018(6)	15.0584(3)
b/Å	14.8952(4)	15.2412(7)	18.5883(4)
c/Å	15.8563(4)	15.9892(7)	28.7616(8)
α/°	78.2080(10)	76.6110(10)	90
β/°	79.0660(10)	77.9940(10)	90
γ/°	69.7140(10)	68.9270(10)	90
Volume/Å^3	3094.52(14)	3177.6(2)	8050.7(3)
Z	2	2	4
ρ_{calc}g/cm^3	1.413	1.428	1.424
μ/mm^{-1}	1.347	1.311	1.641
F(000)	1334.0	1382.0	3524.0
Crystal size/mm^3	0.23 × 0.18 × 0.02	0.1 × 0.08 × 0.02	0.2 × 0.15 × 0.1
Radiation	MoKα (λ = 0.71073)	MoKα (λ = 0.71073)	MoKα (λ = 0.71073)
2Θ range for data collection/°	4.248 to 52.076	4.252 to 52.138	4.382 to 50.086
Index ranges	-17 ≤ h ≤ 17, -18 ≤ k ≤ 18, -18 ≤ l ≤ 19	-17 ≤ h ≤ 15, -18 ≤ k ≤ 18, -19 ≤ l ≤ 19	-16 ≤ h ≤ 17, -22 ≤ k ≤ 22, -34 ≤ l ≤ 34
Reflections collected	46052	44030	50443
Independent reflections	12166 [R_{int} = 0.0386, R_{sigma} = 0.0370]	12380 [R_{int} = 0.0831, R_{sigma} = 0.0952]	14145 [R_{int} = 0.0283, R_{sigma} = 0.0376]
Data/restraints/parameters	12166/18/767	12380/146/868	14145/3/943
Goodness-of-fit on F^2	1.057	1.061	1.057
Final R indexes [I>=2σ (I)]	R_1 = 0.0321, wR_2 = 0.0704	R_1 = 0.0541, wR_2 = 0.1078	R_1 = 0.0358, wR_2 = 0.0992
Final R indexes [all data]	R_1 = 0.0423, wR_2 = 0.0769	R_1 = 0.1016, wR_2 = 0.1307	R_1 = 0.0386, wR_2 = 0.1013
Largest diff. peak/hole / e Å^{-3}	1.10/-1.05	0.70/-1.06	1.14/-1.31
Flack parameter	/	/	-0.001(3)
CCDC number	2178778	2178779	2178780

Table S3. Crystallographic data of complex **3S**, **4R** and **4S**.

Identification code	**3S**	**4R**	**4S**
Empirical formula	$C_{88}H_{85}BBrCl_4DyN_6O_3Si_2$	$C_{88}H_{85}BBrCl_4DyN_6O_3Si_2$	$C_{88}H_{85}BBrCl_4DyN_6O_3Si_2$
Formula weight	1725.82	1725.82	1725.82
Temperature/K	180.0	180.0	180.0
Crystal system	orthorhombic	orthorhombic	orthorhombic
Space group	$P2_12_12_1$	$P2_12_12_1$	$P2_12_12_1$
a/Å	15.0611(3)	14.8456(6)	14.8528(4)
b/Å	18.5926(5)	18.6825(7)	18.6692(4)
c/Å	28.7604(7)	28.9361(9)	28.9684(8)
α/°	90	90	90
β/°	90	90	90
γ/°	90	90	90
Volume/Å^3	8053.6(3)	8025.5(5)	8032.6(4)
Z	4	4	4
ρ_{calc}g/cm^3	1.423	1.428	1.427
μ/mm^{-1}	1.640	1.646	1.644
F(000)	3524.0	3524.0	3524.0
Crystal size/mm^3	0.2 × 0.15 × 0.1	0.3 × 0.25 × 0.2	0.3 × 0.2 × 0.15
Radiation	MoK*α* (*λ* = 0.71073)	MoK*α* (*λ* = 0.71073)	MoK*α* (*λ* = 0.71073)
2*Θ* range for data collection/°	4.488 to 50.086	4.36 to 50.06	3.928 to 50.098
Index ranges	-17 ≤ h ≤ 17, -22 ≤ k ≤ 21, -33 ≤ l ≤ 34	-17 ≤ h ≤ 17, -22 ≤ k ≤ 22, -34 ≤ l ≤ 31	-17 ≤ h ≤ 17, -21 ≤ k ≤ 22, -34 ≤ l ≤ 34
Reflections collected	56587	52797	62832
Independent reflections	14221 [R_{int} = 0.0565, R_{sigma} = 0.0550]	14162 [R_{int} = 0.0738, R_{sigma} = 0.0706]	14166 [R_{int} = 0.0471, R_{sigma} = 0.0467]
Data/restraints/parameters	14221/3/949	14162/15/934	14166/9/943
Goodness-of-fit on F^2	1.050	1.030	1.025
Final R indexes [I>=2*σ* (I)]	R_1 = 0.0429, wR_2 = 0.1097	R_1 = 0.0596, wR_2 = 0.1521	R_1 = 0.0483, wR_2 = 0.1294
Final R indexes [all data]	R_1 = 0.0520, wR_2 = 0.1167	R_1 = 0.0709, wR_2 = 0.1608	R_1 = 0.0530, wR_2 = 0.1332
Largest diff. peak/hole / e Å^{-3}	1.03/-1.44	1.87/-2.44	2.50/-2.21
Flack parameter	-0.007(5)	0.005(6)	0.006(4)
CCDC number	2178781	2178782	2178783

Table S4. Selected bond distances and angles for complex **1** (Å, º).

Dy1-O1	2.141(2)	Dy1-N6	2.680(2)
Dy1-O2	2.138(2)	Dy1-N2	2.678(3)
Dy1-N3	2.695(3)	Dy1-N5	2.646(2)
Dy1-N1	2.676(2)	Dy1-N4	2.642(3)
O1-Dy1-N3	86.34(8)	N1-Dy1-N6	59.71(8)
O1-Dy1-N1	100.53(8)	N1-Dy1-N2	60.90(8)
O1-Dy1-N6	89.40(8)	N6-Dy1-N3	175.65(8)
O1-Dy1-N2	90.66(8)	N2-Dy1-N3	59.74(8)
O1-Dy1-N5	81.70(8)	N2-Dy1-N6	119.49(8)
O1-Dy1-N4	91.22(8)	N5-Dy1-N3	119.60(8)
O2-Dy1-O1	175.53(8)	N5-Dy1-N1	120.13(8)
O2-Dy1-N3	89.93(8)	N5-Dy1-N6	60.50(8)
O2-Dy1-N1	83.47(8)	N5-Dy1-N2	172.36(8)
O2-Dy1-N6	94.36(8)	N4-Dy1-N3	60.90(8)
O2-Dy1-N2	89.59(8)	N4-Dy1-N1	168.22(8)
O2-Dy1-N5	98.05(8)	N4-Dy1-N6	120.16(8)
O2-Dy1-N4	84.81(8)	N4-Dy1-N2	120.33(8)
N1-Dy1-N3	120.25(8)	N4-Dy1-N5	60.45(8)

Table S5. Selected bond distances and angles for complex **2** (Å, º).

Dy1-O1	2.142(4)	Dy1-N3	2.704(4)
Dy1-O2	2.129(4)	Dy1-N6	2.667(5)
Dy1-N1	2.665(4)	Dy1-N2	2.676(4)
Dy1-N5	2.646(4)	Dy1-N4	2.652(4)
O1-Dy1-N1	99.32(14)	N1-Dy1-N6	60.03(14)
O1-Dy1-N5	83.26(14)	N1-Dy1-N2	60.74(14)
O1-Dy1-N3	86.36(14)	N5-Dy1-N1	120.53(14)
O1-Dy1-N6	88.78(15)	N5-Dy1-N3	119.48(14)
O1-Dy1-N2	90.40(14)	N5-Dy1-N6	60.65(14)
O1-Dy1-N4	92.32(14)	N5-Dy1-N2	173.66(15)
O2-Dy1-O1	177.05(15)	N5-Dy1-N4	60.19(14)
O2-Dy1-N1	83.22(14)	N6-Dy1-N3	175.06(14)
O2-Dy1-N5	96.75(14)	N6-Dy1-N2	119.72(14)
O2-Dy1-N3	91.09(14)	N2-Dy1-N3	59.52(14)
O2-Dy1-N6	93.80(14)	N4-Dy1-N1	168.35(14)
O2-Dy1-N2	89.56(14)	N4-Dy1-N3	60.91(14)
O2-Dy1-N4	85.15(14)	N4-Dy1-N6	120.23(14)
N1-Dy1-N3	119.99(13)	N4-Dy1-N2	120.03(14)

Table S6. Selected bond distances and angles for complex **3R** (Å, º).

Dy1-O1	2.131(4)	Dy1-N5	2.720(5)
Dy1-O2	2.138(4)	Dy1-N4	2.632(5)
Dy1-N1	2.628(5)	Dy1-N2	2.660(5)
Dy1-N6	2.650(5)	Dy1-N3	2.608(5)
O1-Dy1-O2	175.4(2)	N1-Dy1-N5	117.30(18)
O1-Dy1-N1	95.67(17)	N1-Dy1-N4	162.24(17)
O1-Dy1-N6	83.84(17)	N1-Dy1-N2	61.60(17)
O1-Dy1-N5	97.34(19)	N6-Dy1-N5	59.78(17)
O1-Dy1-N4	102.07(17)	N6-Dy1-N2	121.73(17)
O1-Dy1-N2	91.50(18)	N4-Dy1-N6	119.68(17)
O1-Dy1-N3	81.89(18)	N4-Dy1-N5	59.93(17)
O2-Dy1-N1	83.91(17)	N4-Dy1-N2	118.07(17)
O2-Dy1-N6	99.87(18)	N2-Dy1-N5	171.15(16)
O2-Dy1-N5	86.86(19)	N3-Dy1-N1	122.53(17)
O2-Dy1-N4	78.47(18)	N3-Dy1-N6	165.55(16)
O2-Dy1-N2	84.29(18)	N3-Dy1-N5	119.96(17)
O2-Dy1-N3	94.49(18)	N3-Dy1-N4	61.68(17)
N1-Dy1-N6	61.19(17)	N3-Dy1-N2	61.09(16)

Table S7. Selected bond distances and angles for complex **3S** (Å, º).

Dy1-O1	2.133(5)	Dy1-N5	2.718(6)
Dy1-O2	2.137(5)	Dy1-N4	2.628(7)
Dy1-N1	2.616(7)	Dy1-N2	2.656(6)
Dy1-N6	2.653(7)	Dy1-N3	2.597(7)
O1-Dy1-N1	95.4(2)	O2-Dy1-N4	78.6(2)
O1-Dy1-O2	175.0(3)	O2-Dy1-N2	84.2(2)
O1-Dy1-N6	84.0(2)	O2-Dy1-N3	94.5(2)
O1-Dy1-N5	97.7(2)	N6-Dy1-N5	59.8(2)
O1-Dy1-N4	102.3(2)	N6-Dy1-N2	121.6(2)
O1-Dy1-N2	91.1(2)	N4-Dy1-N6	119.9(2)
O1-Dy1-N3	81.7(2)	N4-Dy1-N5	60.0(2)
N1-Dy1-N6	61.0(2)	N4-Dy1-N2	118.0(2)
N1-Dy1-N5	117.2(2)	N2-Dy1-N5	171.2(2)
N1-Dy1-N4	162.3(2)	N3-Dy1-N1	122.7(2)
N1-Dy1-N2	61.7(2)	N3-Dy1-N6	165.5(2)
O2-Dy1-N1	83.9(2)	N3-Dy1-N5	119.9(2)
O2-Dy1-N6	99.9(2)	N3-Dy1-N4	61.5(2)
O2-Dy1-N5	87.0(2)	N3-Dy1-N2	61.2(2)

Table S8. Selected bond distances and angles for complex **4R** (Å, º).

Dy1-O1	2.145(7)	Dy1-N6	2.699(8)
Dy1-O2	2.136(7)	Dy1-N1	2.631(9)
Dy1-N4	2.619(9)	Dy1-N2	2.618(9)
Dy1-N3	2.670(9)	Dy1-N5	2.632(10)
O1-Dy1-N4	83.4(3)	O2-Dy1-N1	101.9(3)
O1-Dy1-N3	84.9(3)	O2-Dy1-N2	83.8(3)
O1-Dy1-N6	85.3(3)	O2-Dy1-N5	82.1(3)
O1-Dy1-N1	79.2(3)	N3-Dy1-N6	170.2(3)
O1-Dy1-N2	95.8(3)	N1-Dy1-N3	117.5(3)
O1-Dy1-N5	98.4(3)	N1-Dy1-N6	60.3(3)
N4-Dy1-N3	61.2(3)	N1-Dy1-N5	120.5(3)
N4-Dy1-N6	117.6(3)	N2-Dy1-N4	122.0(3)
N4-Dy1-N1	162.6(3)	N2-Dy1-N3	61.0(3)
N4-Dy1-N5	61.3(3)	N2-Dy1-N6	120.1(3)
O2-Dy1-O1	178.4(4)	N2-Dy1-N1	61.2(3)
O2-Dy1-N4	95.5(3)	N2-Dy1-N5	165.8(3)
O2-Dy1-N3	93.6(3)	N5-Dy1-N3	121.5(3)
O2-Dy1-N6	96.3(3)	N5-Dy1-N6	60.3(3)

Table S9. Selected bond distances and angles for complex **4S** (Å, º).

Dy1-O1	2.141(5)	Dy1-N2	2.623(7)
Dy1-O2	2.140(6)	Dy1-N6	2.702(7)
Dy1-N3	2.670(7)	Dy1-N1	2.628(7)
Dy1-N4	2.632(7)	Dy1-N5	2.634(7)
O1-Dy1-N4	83.3(2)	O2-Dy1-N1	101.8(2)
O1-Dy1-N3	85.2(2)	O2-Dy1-N5	81.7(2)
O1-Dy1-N2	95.7(2)	N3-Dy1-N6	170.2(2)
O1-Dy1-N6	85.0(2)	N2-Dy1-N4	122.0(2)
O1-Dy1-N1	79.0(2)	N2-Dy1-N3	60.8(2)
O1-Dy1-N5	98.3(2)	N2-Dy1-N6	120.2(2)
N4-Dy1-N3	61.3(2)	N2-Dy1-N1	61.2(2)
N4-Dy1-N6	117.4(2)	N2-Dy1-N5	166.0(2)
N4-Dy1-N5	61.3(2)	N1-Dy1-N4	162.2(2)
O2-Dy1-O1	179.1(3)	N1-Dy1-N3	117.4(2)
O2-Dy1-N4	96.0(2)	N1-Dy1-N6	60.4(2)
O2-Dy1-N3	94.0(3)	N1-Dy1-N5	120.5(2)
O2-Dy1-N2	84.3(2)	N5-Dy1-N3	121.6(2)
O2-Dy1-N6	95.8(3)	N5-Dy1-N6	60.1(2)

Table S10. The CShM values calculated by SHAPE 2.1 for **1** and **2**.[8, 9]

Central atom	Coordination Geometry	**1**	**2**
Dy	Octagon (D_{8h})	29.252	29.595
	Heptagonal pyramid (C_{7v})	20.877	21.260
	Hexagonal bipyramid (D_{6h})	**1.347**	**1.281**
	Cube (O_h)	9.676	9.623
	Square antiprism (D_{4d})	17.729	17.739
	Triangular dodecahedron (D_{2d})	15.216	15.083
	Johnson gyrobifastigium J26 (D_{2d})	7.660	7.831
	Biaugmented trigonal prism J50 (C_{2v})	16.592	16.600
	Biaugmented trigonal prism (C_{2v})	16.361	16.467
	Snub diphenoid J84 (D_{2d})	16.559	16.674
	Triakis tetrahedron (T_d)	10.524	10.461
	Elongated trigonal bipyramid (D_{3h})	20.998	21.280

Table S11. The CShM values calculated by SHAPE 2.1 for **3R** and **3S**.[8, 9]

Central atom	Coordination Geometry	**3R**	**3S**
Dy	Octagon (D_{8h})	30.575	30.493
	Heptagonal pyramid (C_{7v})	21.613	21.564
	Hexagonal bipyramid (D_{6h})	**1.977**	**1.964**
	Cube (O_h)	10.278	10.240
	Square antiprism (D_{4d})	16.775	16.750
	Triangular dodecahedron (D_{2d})	14.584	14.592
	Johnson gyrobifastigium J26 (D_{2d})	6.138	6.154
	Biaugmented trigonal prism J50 (C_{2v})	15.410	15.388
	Biaugmented trigonal prism (C_{2v})	15.260	15.272
	Snub diphenoid J84 (D_{2d})	15.288	15.264
	Triakis tetrahedron (T_d)	10.988	10.933
	Elongated trigonal bipyramid (D_{3h})	21.007	20.908

Table S12. The CShM values calculated by SHAPE 2.1 for **4R** and **4S**.[8, 9]

Central atom	Coordination Geometry	**4R**	**4S**
Dy	Octagon (D_{8h})	30.728	30.752
	Heptagonal pyramid (C_{7v})	22.266	22.180
	Hexagonal bipyramid (D_{6h})	**1.897**	**1.909**
	Cube (O_h)	10.255	10.347
	Square antiprism (D_{4d})	16.540	16.604
	Triangular dodecahedron (D_{2d})	14.328	14.386
	Johnson gyrobifastigium J26 (D_{2d})	6.155	6.119
	Biaugmented trigonal prism J50 (C_{2v})	15.076	15.104
	Biaugmented trigonal prism (C_{2v})	14.949	14.957
	Snub diphenoid J84 (D_{2d})	15.170	15.204
	Triakis tetrahedron (T_d)	10.940	11.035
	Elongated trigonal bipyramid (D_{3h})	21.205	21.221

Table S13. Selected intermolecular interactions for **1**[a].

		Length/ Å	Length-VdW/ Å
π···π	C18···C3	3.372	-0.028
	C32···C34	3.395	-0.005
C-H···π	C39-H39···C41	2.782	-0.118
	C39-H39···C49	2.877	-0.023
	C7-H7···C50	2.894	-0.006
	C45-H45···C40	2.814	-0.086
	C3-H3···C62	2.831	-0.069
	C52-H52···C26	2.599	-0.301
	C52-H52···C48	2.601	-0.299
C-H···O	C35-H35···O6	2.538	-0.182
	C13-H13···O6	2.665	-0.055
	C18-H18···O5	2.719	-0.001
	C18-H18···O4	2.513	-0.207
	C58-H58···O4	2.691	-0.029
	C62-H62···O5	2.461	-0.259
	C34-H34···O4	2.705	-0.015
	C51-H51···O3	2.47	-0.25
C-H···N	C24-H24···N7	2.613	-0.137
C-H···Si	C45-H45···Si1	3.245	-0.055

[a] Short contacts are given for distances inferior to the sum of van der Waals radii.

Table S14. Selected intermolecular interactions for **2**[a].

		Length/ Å	Length-VdW/ Å
C-H···π	C29-H29···C66	2.746	-0.154
	C29-H29···C45	2.876	-0.024
	C34-H34···C36	2.647	-0.253
	C34-H34···C52	2.654	-0.246
	C35-H35···C18	2.885	-0.015
	C53-H53···C48	2.893	-0.007
	C67-H67C···C33	2.852	-0.048
C-H···F	C41-H41···F6	2.278	-0.392
	C25-H25···F4	2.507	-0.163
	C60-H60···F4	2.488	-0.182
	C38-H38···F5	2.479	-0.191
	C42-H42···F5	2.531	-0.139
C-H···O	C67-H67A···O4	2.008	-0.712
	C48-H48···O5	2.705	-0.015
C-H···N	C30-H30···N7	2.621	-0.129
C-H···Si	C35-H35···Si2	3.264	-0.036

[a] Short contacts are given for distances inferior to the sum of van der Waals radii.

Table S15. Selected intermolecular interactions for **3R**[a].

		Length/ Å	Length-VdW/ Å
C-H···π	C20-H20···C72	2.847	-0.053
	C20-H20···C65	2.814	-0.086
	C20-H20···C69	2.837	-0.063
	C46-H46···C11	2.747	-0.153
	C81-H81···C73	2.859	-0.041
	C81-H81···C39	2.868	-0.032
	C50-H50···C7	2.866	-0.034
	C18-H18···C49	2.844	-0.056
	C18-H18···C31	2.845	-0.055
	C32-H32···C38	2.892	-0.008
	C32-H32···C33	2.883	-0.017
	C9-H9···C68	2.813	-0.087
	C23-H23A···C17	2.844	-0.056
	C45-H45···C83	2.85	-0.05
	C83-H83···C45	2.863	-0.037
	C87-H87B···C47	2.795	-0.105
C-H···Cl	C69-H69···Cl1	2.939	-0.011
	C19-H19···Cl4	2.684	-0.266
C-H···Br	C60-H60B···Br1	3.008	-0.042

[a] Short contacts are given for distances inferior to the sum of van der Waals radii.

Table S16. Selected intermolecular interactions for **3S**[a].

		Length/ Å	Length-VdW/ Å
C-H···π	C50-H50···C51	2.841	-0.059
	C50-H50···C67	2.798	-0.102
	C50-H50···C35	2.81	-0.09
	C86-H86···C7	2.741	-0.159
	C5-H5···C77	2.873	-0.027
	C5-H5···C41	2.866	-0.034
	C11-H11···C9	2.872	-0.028
	C20-H20···C55	2.841	-0.059
	C20-H20···C65	2.859	-0.041
	C70-H70···C39	2.894	-0.006
	C79-H79···C74	2.822	-0.078
	C60-H60A···C63	2.831	-0.069
	C45-H45···C81	2.869	-0.031
	C81-H81···C45	2.878	-0.022
	C43-H43A···C4	2.884	-0.016
	C87-H87B···C53	2.806	-0.094
C-H···Cl	C19-H19···Cl4	2.695	-0.255
C-H···Br	C80-H80A···Br1	3.000	-0.05

[a] Short contacts are given for distances inferior to the sum of van der Waals radii.

Table S17. Selected intermolecular interactions for **4R**[a].

		Length/ Å	Length-VdW/ Å
C-H···π	C22-H22···C21	2.755	-0.145
	C36-H36···C47	2.785	-0.115
	C36-H36···C66	2.879	-0.021
	C36-H36···C73	2.879	-0.021
	C38-H38A···C13	2.883	-0.017
	C13-H13···C79	2.753	-0.147
	C87-H87···C49	2.886	-0.014
	C39-H39···C79	2.768	-0.132
	C27-H27···C33	2.855	-0.045
	C27-H27···C34	2.824	-0.076
	C32-H32···C65	2.815	-0.085
	C41-H41···C69	2.864	-0.036
	C80-H80···C9	2.899	-0.001
	C85-H85B···C59	2.895	-0.005
C-H···Cl	C88-H88···Cl1	2.649	-0.301
C-H···Br	C68-H68···Br1	2.713	-0.337
	C84-H84···Br1	3.027	-0.023

[a] Short contacts are given for distances inferior to the sum of van der Waals radii.

Table S18. Selected intermolecular interactions for **4S**[a].

		Length/ Å	Length-VdW/ Å
C-H···π	C28-H28···C12	2.739	-0.161
	C46-H46···C50	2.802	-0.098
	C46-H46···C65	2.891	-0.009
	C46-H46···C70	2.886	-0.014
	C39-H39B···C25	2.889	-0.011
	C25-H25···C82	2.731	-0.169
	C84-H84···C44	2.896	-0.004
	C35-H35···C82	2.818	-0.082
	C22-H22···C33	2.842	-0.058
	C22-H22···C34	2.861	-0.039
	C15-H15···C26	2.894	-0.006
	C32-H32···C63	2.868	-0.032
	C48-H48···C77	2.822	-0.078
	C75-H75···C13	2.888	-0.012
	C87-H87A···C52	2.877	-0.023
	C87-H87B···C60	2.89	-0.01
C-H···Cl	C83-H83···Cl1	2.65	-0.3
C-H···Br	C88-H88A···Br1	2.941	-0.109
	C85-H85···Br1	3.049	-0.001
	C68-H68···Br1	2.72	-0.33

[a] Short contacts are given for distances inferior to the sum of van der Waals radii.

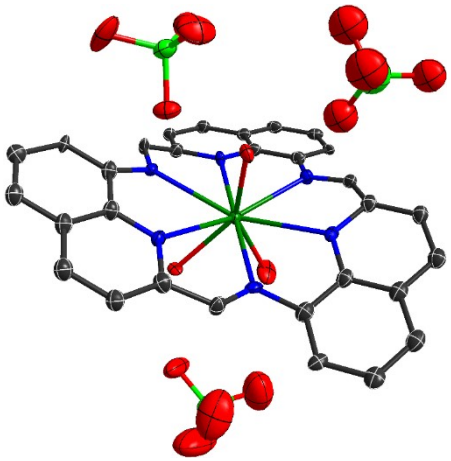

Figure S10. Thermal ellipsoid representations (30% probability) of the molecular structure of precursor **A**. Dy, dark green; Cl, bright green; O, red; N, blue; C, grey. For clarity, H atoms and lattice solvents are omitted.

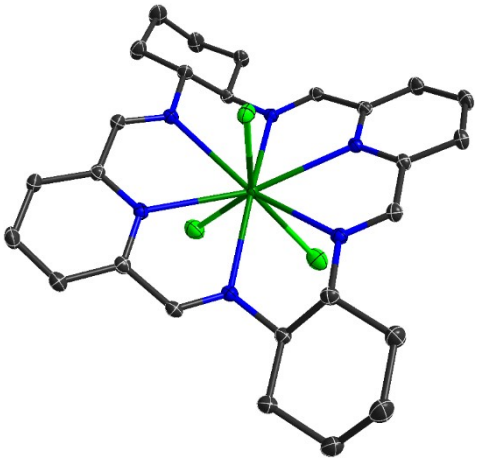

Figure S11. Thermal ellipsoid representations (30% probability) of the molecular structure of precursor (RRRR)-**B**. Dy, dark green; Cl, bright green; N, blue; C, grey. For clarity, H atoms and lattice solvents are omitted.

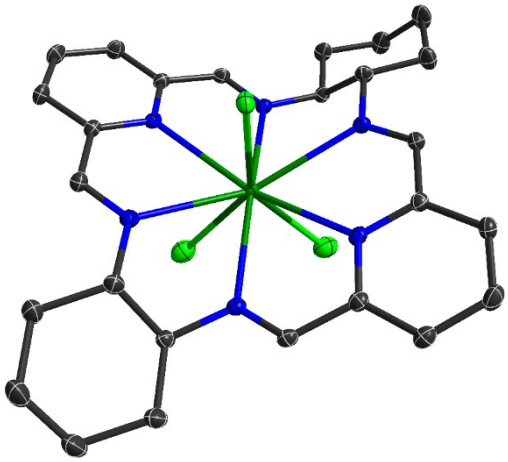

Figure S12. Thermal ellipsoid representations (30% probability) of the molecular structure of precursor (SSSS)-**B**. Dy, dark green; Cl, bright green; N, blue; C, grey. For clarity, H atoms and lattice solvents are omitted.

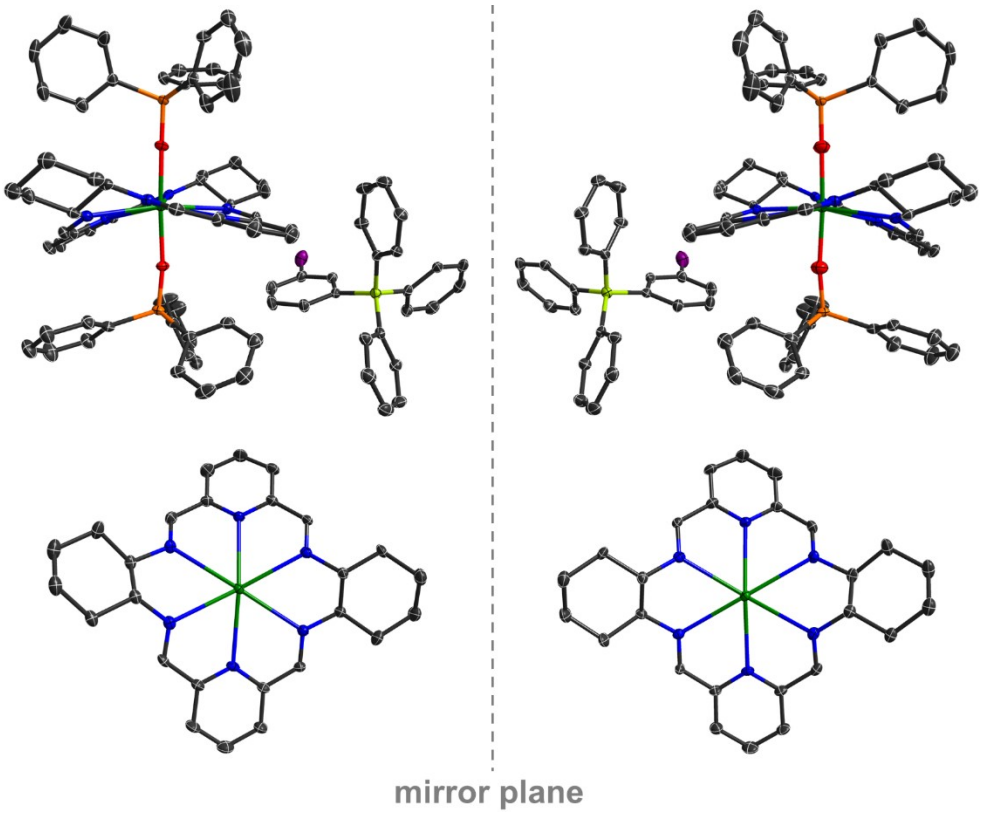

Figure S13 Thermal ellipsoid representations (30% probability) of the molecular structures (upper) and equatorial coordination environment (bottom) of **3R** (left) and **3S** (right). Dy, dark green; Br, violet; Si, orange; O, red; N, blue; C, grey; B, lime. For clarity, H atoms and lattice solvents are omitted.

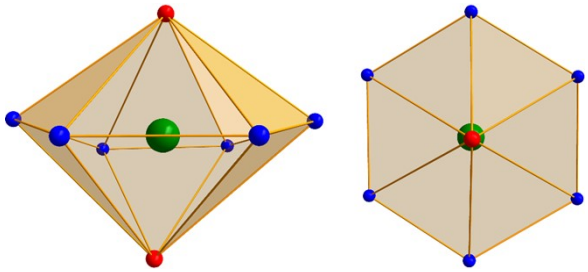

Figure S14. Polyhedron viewed from the side (left) and the top (right) showing hexagonal bipyramidal geometry of complex **2**. Dy, dark green; O, red; N, blue.

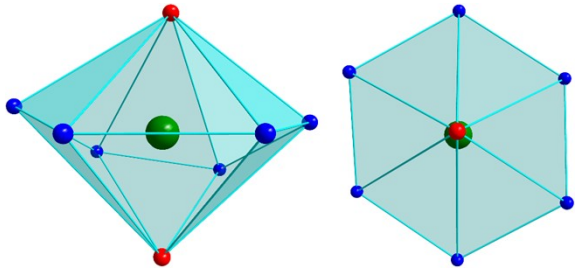

Figure S15 Polyhedron viewed from the side (left) and the top (right) showing hexagonal bipyramidal geometry of complex **3R**. Dy, dark green; O, red; N, blue.

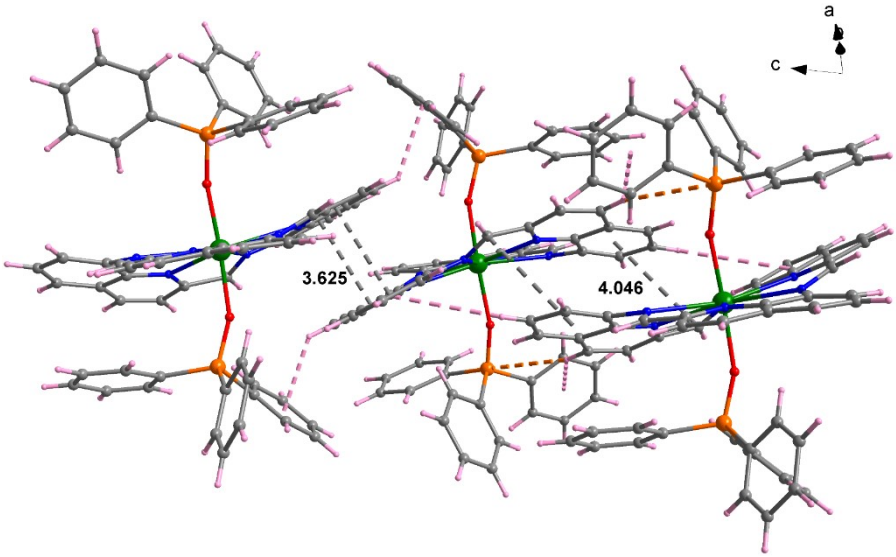

Figure S16. Intermolecular interactions (inferior to the sum of van der Waals radii) of **1**, viewed along the specific direction. Dy dark green; Si, orange; N blue; O red; C grey; H rose. Counter anions and lattice solvents are omitted for clarity. Short contacts are shown as dashed lines: π···π grey; C-H···Si orange; C-H···π rose.

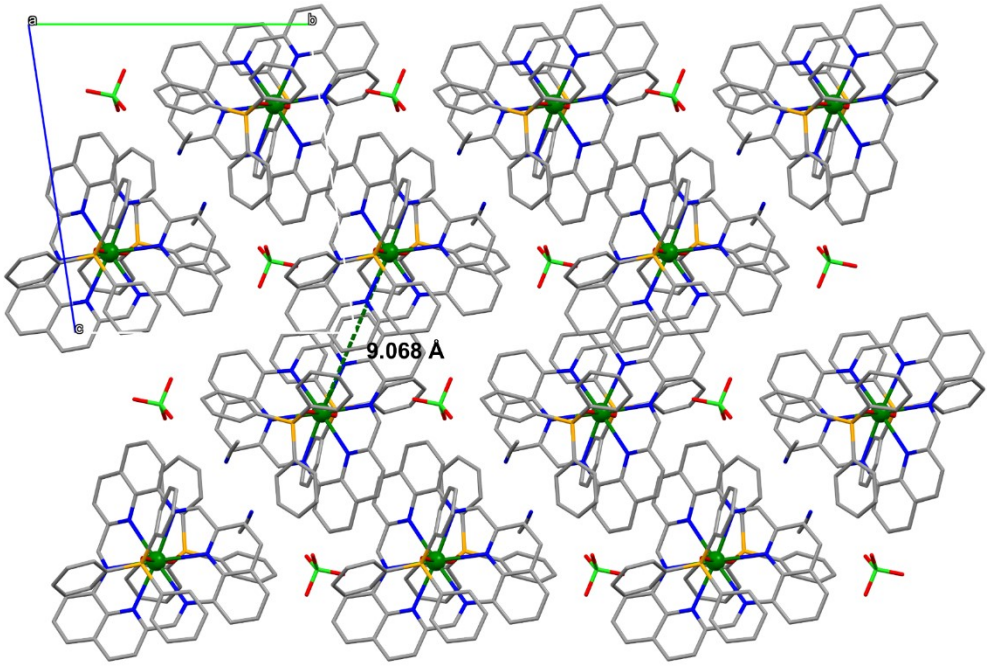

Figure S17. The crystal packing of **1** viewed along *a* axis with the shortest Dy···Dy distance of 9.068 Å. Hydrogen atoms are omitted for clarity. Dy dark green; Cl, bright green; Si, orange; N blue; O red; C grey.

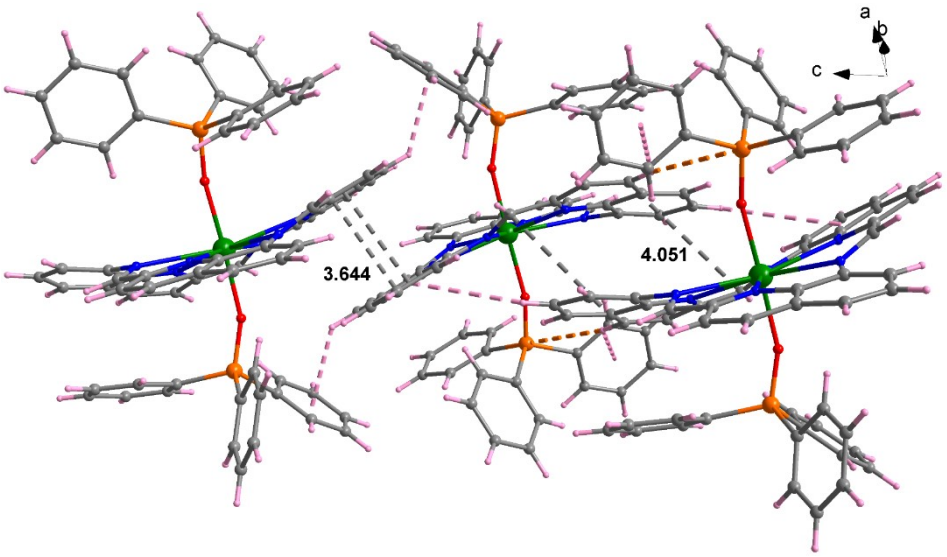

Figure S18. Intermolecular interactions (inferior to the sum of van der Waals radii) of **2**, viewed along the specific direction. Dy dark green; Si, orange; N blue; O red; C grey; H rose. Counter anions and lattice solvents are omitted for clarity. Short contacts are shown as dashed lines: π···π grey; C-H···Si orange; C-H···π rose.

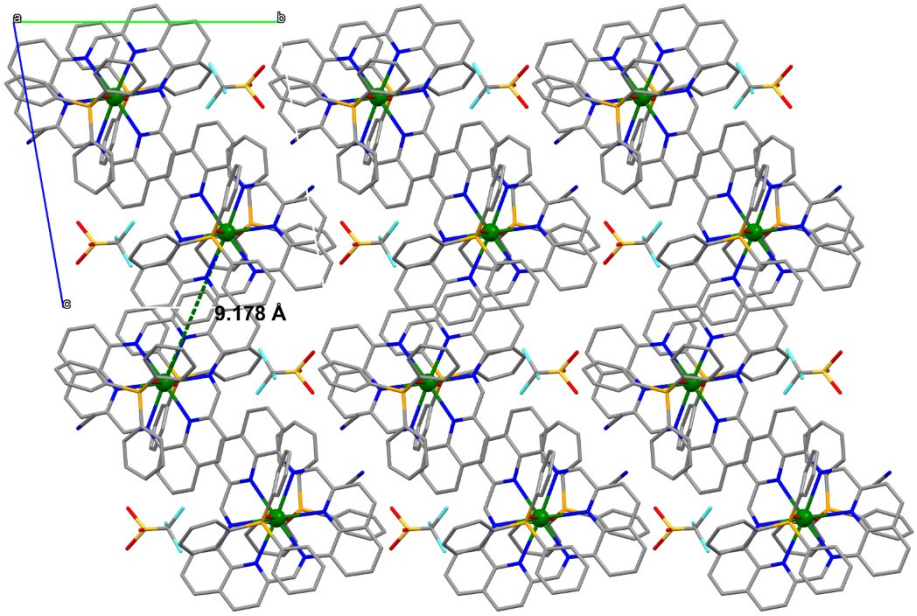

Figure S19. The crystal packing of **2** viewed along *a* axis with the shortest Dy···Dy distance of 9.178 Å. Hydrogen atoms are omitted for clarity. Dy, dark green; Si, orange; S, yellow; F, turquoise; O, red; N, blue; C, grey.

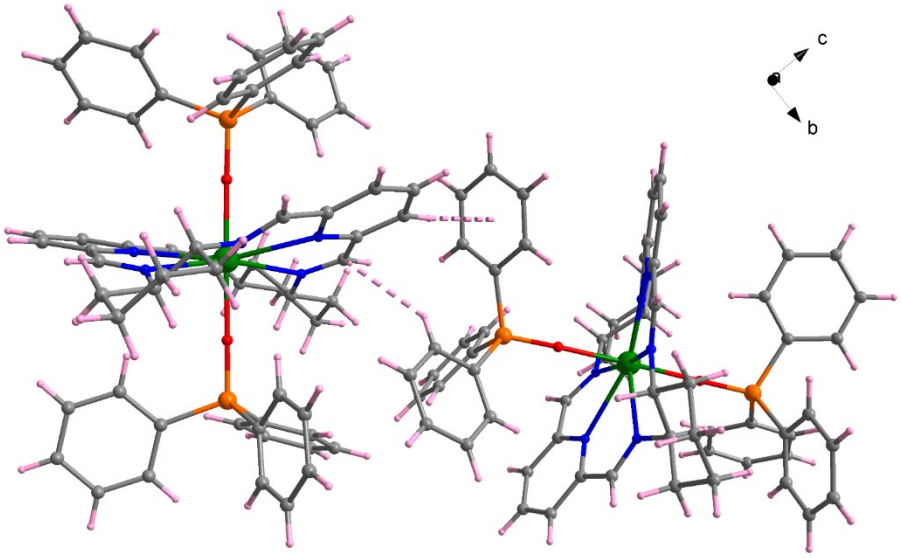

Figure S20. Intermolecular interactions (inferior to the sum of van der Waals radii) of **3R**, viewed along the specific direction. Dy, dark green; Si, orange; O, red; N, blue; C, grey; H rose. Counter anions and lattice solvents are omitted for clarity. Short contacts are shown as dashed lines: C-H···π rose.

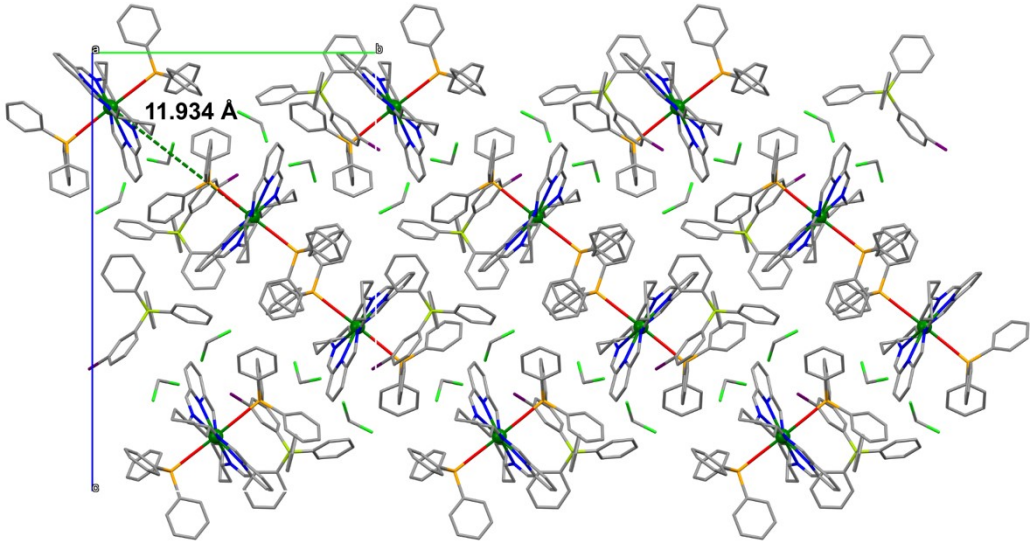

Figure S21. The crystal packing of **3R** viewed along *a* axis with the shortest Dy···Dy distance of 11.934 Å. Hydrogen atoms are omitted for clarity. Dy, dark green; Br, violet; Cl, bright green; Si, orange; O, red; N, blue; C, grey; B, lime.

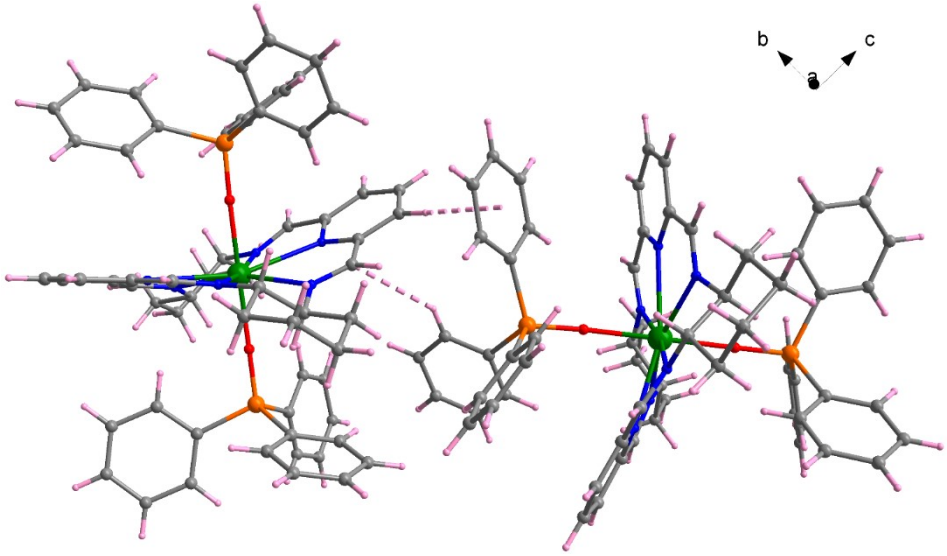

Figure S22. Intermolecular interactions (inferior to the sum of van der Waals radii) of **3S**, viewed along the specific direction. Dy, dark green; Si, orange; O, red; N, blue; C, grey; H rose. Counter anions and lattice solvents are omitted for clarity. Short contacts are shown as dashed lines: C-H···π rose.

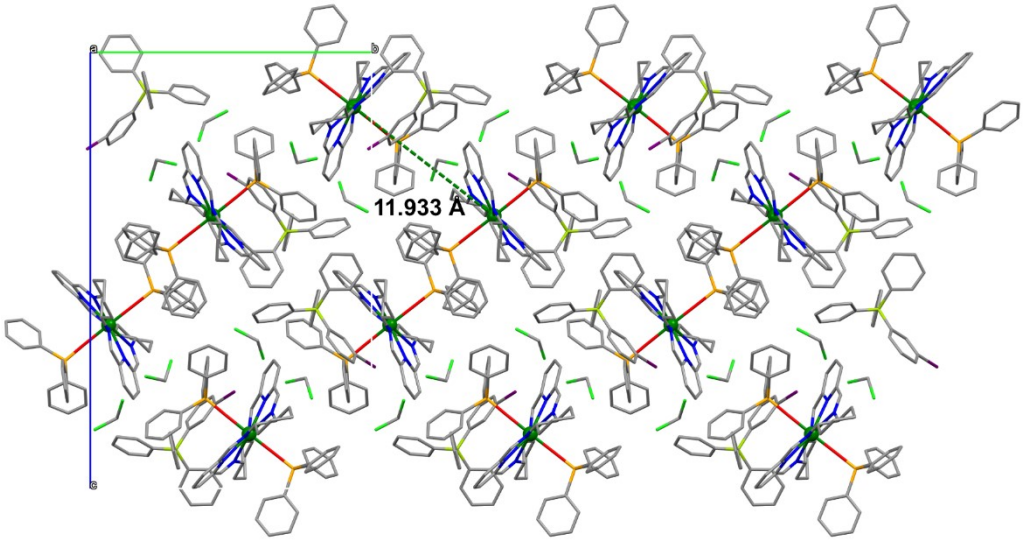

Figure S23. The crystal packing of **3S** viewed along *a* axis with the shortest Dy···Dy distance of 11.933 Å. Hydrogen atoms are omitted for clarity. Dy, dark green; Br, violet; Cl, bright green; Si, orange; O, red; N, blue; C, grey; B, lime.

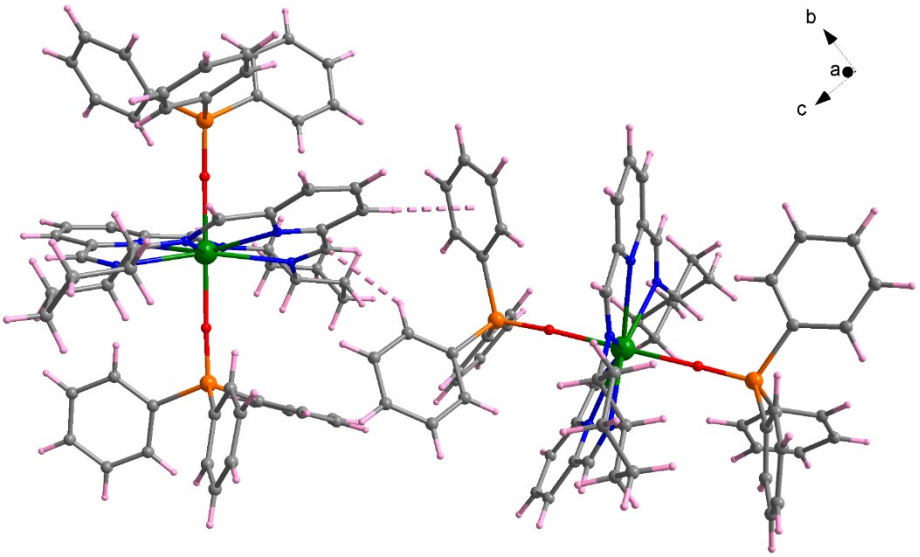

Figure S24. Intermolecular interactions (inferior to the sum of van der Waals radii) of **4R**, viewed along the specific direction. Dy, dark green; Si, orange; O, red; N, blue; C, grey; H rose. Counter anions and lattice solvents are omitted for clarity. Short contacts are shown as dashed lines: C-H···π rose.

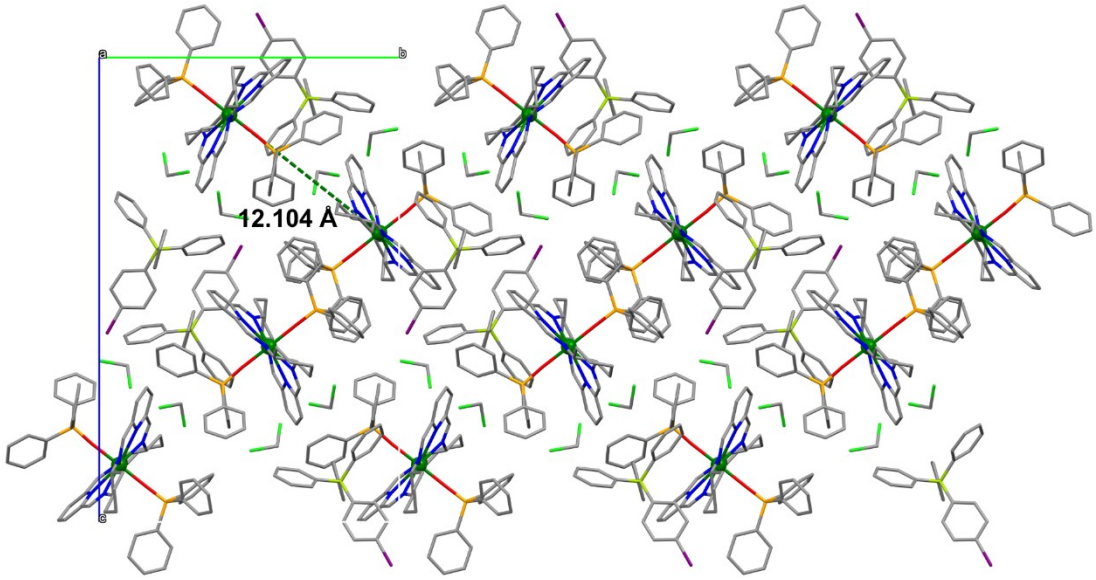

Figure S25. The crystal packing of **4R** viewed along *a* axis with the shortest Dy···Dy distance of 12.104 Å. Hydrogen atoms are omitted for clarity. Dy, dark green; Br, violet; Cl, bright green; Si, orange; O, red; N, blue; C, grey; B, lime.

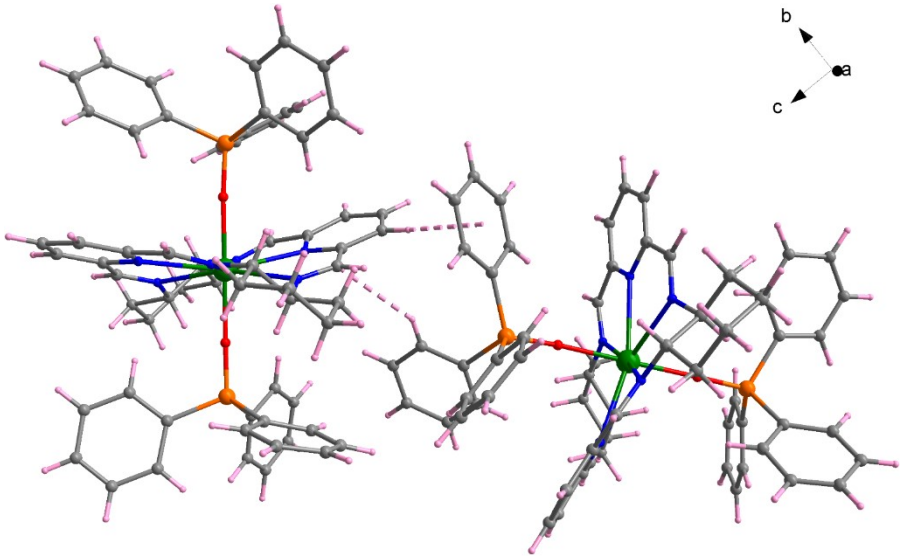

Figure S26. Intermolecular interactions (inferior to the sum of van der Waals radii) of **4S**, viewed along the specific direction. Dy, dark green; Si, orange; O, red; N, blue; C, grey; H rose. Counter anions and lattice solvents are omitted for clarity. Short contacts are shown as dashed lines: C-H···π rose.

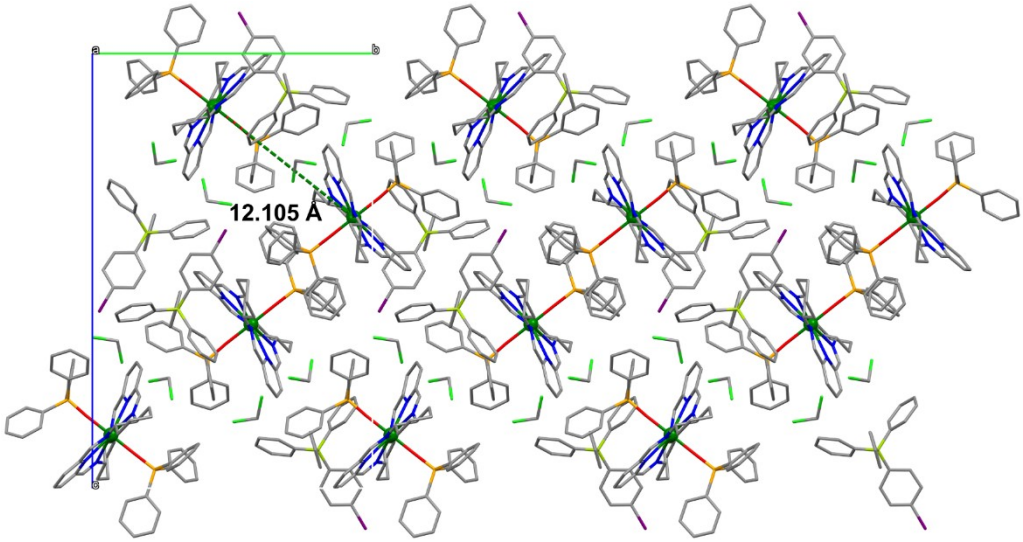

Figure S27. The crystal packing of **4S** viewed along *a* axis with the shortest Dy···Dy distance of 12.105 Å. Hydrogen atoms are omitted for clarity. Dy, dark green; Br, violet; Cl, bright green; Si, orange; O, red; N, blue; C, grey; B, lime.

IV. Magnetic characterization

Table S19 Relaxation fitting parameters for **1** obtained from CCFIT2.

T / K	χ_S / cm^3 mol^{-1}	χ_T / cm^3 mol^{-1}	τ / s	α	Residual
2	0.11906	10.1427	0.54772	0.30849	0.09537
3	0.10895	6.75639	0.44265	0.29417	0.07862
5	0.09675	4.00675	0.32393	0.2723	0.03249
7	0.08666	2.84774	0.25927	0.26308	0.01925
10	0.07329	1.98996	0.20575	0.26943	0.01302
15	0.07219	1.33301	0.14616	0.23648	0.01475
20	0.06333	0.9756	0.09515	0.18212	0.01644
25	0.05994	0.76791	0.0633	0.1359	0.00904
30	0.05667	0.63461	0.04339	0.10603	0.00588
35	0.05077	0.55202	0.03167	0.09692	0.0027
40	0.04156	0.48388	0.02242	0.10274	0.0034
45	0.04927	0.4209	0.01676	0.04866	9.36E-04
50	0.04379	0.38284	0.01265	0.05318	0.00101
55	0.0382	0.34571	0.00958	0.04723	7.26E-04
60	0.03378	0.31644	0.00703	0.04337	7.66E-04
65	0.04072	0.29102	0.0053	0.03395	6.37E-04
70	0.03109	0.27194	0.004	0.03892	0.00111
75	0.02583	0.25384	0.00244	0.07466	0.00103
78	0.03021	0.24575	0.00186	0.06324	6.25E-04
81	0.03094	0.23649	0.00131	0.03598	5.28E-04
83	0.02964	0.2284	9.63E-04	0.06067	4.44E-04
85	0.02536	0.22413	7.58E-04	0.03881	5.09E-04
86	0.04117	0.21952	6.92E-04	1.59E-06	4.15E-04
87	0.03647	0.21887	5.88E-04	1.78E-06	4.10E-04
88	0.0401	0.21304	4.99E-04	2.31E-06	5.44E-04
89	0.04434	0.21239	4.29E-04	3.01E-06	8.30E-04
90	0.03321	0.20756	3.67E-04	5.16E-06	5.19E-04
91	0.05027	0.20332	3.24E-04	6.42E-06	6.40E-04
92	0.04911	0.20513	2.79E-04	6.35E-06	5.02E-04
93	0.04493	0.20324	2.38E-04	7.84E-06	0.00102
94	0.02939	0.19949	1.99E-04	1.06E-05	5.65E-04
95	0.03645	0.19864	1.62E-04	1.13E-05	2.58E-04
96	0.04252	0.19482	1.42E-04	1.55E-05	9.73E-04
97	0.04312	0.19576	1.19E-04	2.53E-05	5.23E-04
98	0.047	0.19353	9.91E-05	2.99E-05	5.65E-04
99	6.46E-16	0.19405	8.19E-05	0.10885	4.17E-04

Table S20 Relaxation fitting parameters for **2** obtained from CCFIT2.

T / K	χ_S / cm^3 mol^{-1}	χ_T / cm^3 mol^{-1}	τ / s	α	Residual
2	0.04132	11.6023	3.72437	0.40536	0.00191
3	0.04598	7.60047	2.69417	0.39036	0.00299
5	0.03937	4.327	1.52678	0.36951	0.00112
7	0.0341	3.12381	1.16424	0.37865	0.00163
10	0.03669	2.22918	0.86632	0.37315	0.00437
15	0.04748	1.3896	0.42352	0.28598	0.01301
20	0.05091	0.97318	0.22078	0.18464	0.00971
25	0.04941	0.75248	0.13083	0.12131	0.00538
30	0.04594	0.62802	0.08321	0.11067	0.00507
35	0.03867	0.54288	0.05564	0.08408	0.00208
40	0.03586	0.47158	0.03679	0.0703	0.00113
45	0.0346	0.41687	0.02512	0.05102	4.44E-04
50	0.03189	0.37364	0.01759	0.04213	2.28E-04
55	0.03065	0.3396	0.01233	0.0392	2.56E-04
60	0.02647	0.31345	0.00827	0.05706	8.56E-04
65	0.02833	0.28618	0.00548	0.02436	5.05E-04
70	0.02453	0.26632	0.00312	0.04867	2.18E-04
75	0.02568	0.24789	0.00162	0.02967	4.68E-04
78	0.02171	0.23842	9.92E-04	0.05019	2.73E-04
81	0.01817	0.23013	5.75E-04	0.07413	1.93E-04
83	0.01292	0.22465	4.10E-04	0.08528	4.68E-04
85	0.02011	0.21862	3.08E-04	0.06286	2.64E-04
86	0.02356	0.21535	2.64E-04	0.05759	4.12E-04
87	0.00968	0.21373	2.01E-04	0.08479	2.96E-04
88	0.00593	0.21121	1.79E-04	0.07008	2.74E-04
89	0.03278	0.2063	1.59E-04	9.86E-16	2.54E-04
90	0.04046	0.20511	1.44E-04	1.36E-15	3.58E-04
91	0.05526	0.20293	1.30E-04	1.67E-15	1.74E-04
92	0.04095	0.20115	1.06E-04	1.91E-15	2.74E-04
93	0.05219	0.19965	9.08E-05	2.41E-15	1.85E-04
94	0.01908	0.19669	7.28E-05	1.83E-15	1.95E-04
95	0.0499	0.19421	6.09E-05	2.02E-15	1.79E-04
96	0.05967	0.19222	5.19E-05	2.56E-15	1.97E-04
97	0.06085	0.19015	4.34E-05	3.05E-15	1.66E-04
98	0.08038	0.18833	3.67E-05	4.27E-15	3.16E-04
99	2.66E-16	0.18883	3.06E-05	3.49E-15	1.91E-04

Table S21 Relaxation fitting parameters for **3R** obtained from CCFIT2.

T / K	χ_S / cm^3 mol^{-1}	χ_T / cm^3 mol^{-1}	τ / s	α	Residual
2	0.04006	7.01892	0.03639	0.29128	0.00609
3	0.03526	4.7305	0.03381	0.27512	0.00503
4	0.03178	3.55757	0.0315	0.26133	0.00448
5	0.02917	2.85748	0.02954	0.24714	0.00451
6	0.02838	2.38015	0.02764	0.2337	0.00487
7	0.02531	2.03341	0.02557	0.21985	0.00447
8	0.02474	1.77179	0.02349	0.20567	0.00398
10	0.02185	1.40565	0.01943	0.18167	0.00343
12	0.02023	1.16497	0.01587	0.15988	0.00249
14	0.01841	0.99224	0.01291	0.14239	0.00173
16	0.01846	0.86622	0.01065	0.12779	0.00127
19	0.01423	0.72629	0.0081	0.11618	7.34E-04
22	0.01411	0.62562	0.00643	0.10749	5.94E-04
25	0.01408	0.54864	0.00525	0.09693	4.39E-04
28	0.01307	0.48815	0.00436	0.08714	4.26E-04
31	0.0126	0.4414	0.00369	0.08807	5.43E-04
34	0.01171	0.40201	0.00311	0.08074	2.01E-04
37	0.01291	0.36941	0.00269	0.07305	8.71E-05
40	0.0101	0.34232	0.00229	0.07184	1.49E-04
43	0.0086	0.31846	0.00197	0.07234	1.15E-04
46	0.01007	0.29789	0.00173	0.0598	1.25E-04
49	0.0084	0.27993	0.00151	0.0604	1.11E-04
52	0.0062	0.26456	0.00128	0.07077	2.32E-04
55	0.00819	0.24988	0.00112	0.0641	1.33E-04
58	0.00771	0.23708	9.43E-04	0.06176	8.84E-05
61	0.01075	0.22566	8.07E-04	0.04783	1.04E-04
62	0.01019	0.22153	7.43E-04	0.05011	1.64E-04
63	0.00387	0.2187	6.55E-04	0.07946	1.73E-04
64	0.00368	0.2155	6.16E-04	0.06854	1.74E-04
65	0.00595	0.21153	5.79E-04	0.0575	9.12E-05
66	0.01133	0.20885	5.46E-04	0.04864	1.22E-04
67	8.22E-04	0.20557	4.64E-04	0.08005	9.51E-05
68	0.00635	0.20194	4.30E-04	0.06298	8.87E-05
69	0.0039	0.19885	3.79E-04	0.07005	9.35E-05
70	0.00106	0.19504	3.39E-04	0.06756	1.10E-04
71	1.01E-08	0.19206	2.97E-04	0.09006	1.24E-04
72	1.43E-08	0.18959	2.68E-04	0.08181	8.84E-05
73	1.83E-08	0.18638	2.38E-04	0.08915	1.33E-04
74	2.59E-08	0.18405	2.08E-04	0.09213	2.44E-04
75	3.79E-08	0.18183	1.73E-04	0.1026	1.82E-04
76	5.92E-08	0.17875	1.51E-04	0.09183	8.24E-05

77	8.69E-08	0.17667	1.31E-04	0.1035	2.49E-04
78	1.39E-07	0.17449	1.09E-04	0.09818	1.24E-04
79	2.01E-07	0.1722	9.61E-05	0.09928	6.41E-05
80	2.62E-07	0.16998	8.29E-05	0.11935	1.80E-04
81	4.28E-07	0.16668	6.74E-05	0.046	1.78E-04
82	5.07E-07	0.16556	5.51E-05	0.07479	1.09E-04
83	7.06E-07	0.16419	4.45E-05	0.05812	1.04E-04

Table S22 Relaxation fitting parameters for **3S** obtained from CCFIT2.

T / K	χ_S / cm^3 mol^{-1}	χ_T / cm^3 mol^{-1}	τ / s	α	Residual
2	0.04749	7.50694	0.09394	0.22202	0.01295
3	0.03809	4.954	0.07704	0.19088	0.00858
5	3.94E-17	2.94334	0.059	0.18658	0.01167
8	8.66E-17	1.80259	0.04338	0.15696	0.00259
11	1.15E-16	1.30862	0.03365	0.15149	0.00268
16	1.37E-16	0.89137	0.02214	0.12223	0.00177
21	2.96E-16	0.67481	0.01541	0.09974	0.0019
26	4.74E-16	0.54155	0.01131	0.08455	0.00134
31	7.40E-16	0.45361	0.00852	0.07469	0.00125
36	1.33E-15	0.3925	0.00662	0.06835	0.00163
41	1.56E-15	0.34108	0.00511	0.05553	8.25E-04
46	3.90E-15	0.30623	0.00406	0.0526	0.00119
51	9.31E-15	0.27581	0.00324	0.04418	6.94E-04
56	1.26E-14	0.24966	0.00253	0.03489	3.67E-04
61	1.20E-14	0.22992	0.00196	0.04496	4.82E-04
66	1.08E-14	0.21403	0.00134	0.05246	8.32E-04
70	1.46E-14	0.19964	9.44E-04	0.03383	4.14E-04
73	1.90E-14	0.19187	6.89E-04	0.03765	2.47E-04
76	1.42E-14	0.1842	4.72E-04	0.03067	8.70E-04
78	1.62E-14	0.1816	3.55E-04	0.05062	4.89E-04
80	2.64E-14	0.17492	2.62E-04	0.01523	2.01E-04
81	7.26E-14	0.17384	2.25E-04	0.05586	7.48E-04
82	1.34E-13	0.1696	1.98E-04	0.00769	3.26E-04
83	6.55E-14	0.16774	1.61E-04	0.01521	1.45E-04
84	1.13E-13	0.16455	1.40E-04	0.00153	6.58E-04
85	3.16E-12	0.16388	1.18E-04	0.08319	5.82E-04
86	4.30E-12	0.16305	9.88E-05	0.05435	8.38E-04
87	5.85E-12	0.16233	8.26E-05	0.05169	0.00101
88	1.09E-11	0.15846	6.92E-05	6.39E-16	4.14E-04
89	1.56E-11	0.15536	5.73E-05	8.14E-16	8.30E-04
90	2.07E-11	0.15619	4.81E-05	8.32E-16	4.74E-04

Table S23 Relaxation fitting parameters for **4R** obtained from CCFIT2.

T / K	χ_S / cm^3 mol^{-1}	χ_T / cm^3 mol^{-1}	τ / s	α	Residual
2	0.03929	7.14749	0.07467	0.27297	0.00929
3	0.02871	4.8198	0.06954	0.26085	0.0057
5	0.02294	2.93617	0.05943	0.2342	0.00411
8	0.01652	1.81431	0.04282	0.19024	0.00437
11	0.01817	1.29706	0.03001	0.15139	0.0042
16	0.01587	0.87905	0.01733	0.11463	0.00178
21	0.01208	0.66564	0.01112	0.09423	0.00155
26	0.01341	0.53148	0.00777	0.0728	8.75E-04
31	0.01208	0.44463	0.00572	0.06676	8.81E-04
36	0.01489	0.383	0.00433	0.05105	2.88E-04
41	0.01317	0.33497	0.00331	0.03594	1.98E-04
46	0.00888	0.29954	0.00254	0.04781	6.12E-04
51	0.01034	0.27108	0.002	0.03314	2.64E-04
56	0.01053	0.24534	0.00156	0.02949	3.61E-04
61	0.00522	0.22672	0.00115	0.05172	3.48E-04
66	0.00699	0.21112	8.23E-04	0.02762	6.33E-04
70	0.01274	0.19933	6.00E-04	0.02663	3.55E-04
73	0.01708	0.18779	4.47E-04	0.03178	0.00101
76	0.00708	0.18014	2.97E-04	0.02803	3.79E-04
78	3.48E-11	0.17855	2.09E-04	0.06377	8.68E-04
80	4.55E-11	0.17361	1.56E-04	0.06619	1.77E-04
81	6.18E-11	0.17047	1.27E-04	0.06871	4.78E-04
82	1.11E-10	0.16661	1.12E-04	0.00969	0.00198
83	5.63E-12	0.16612	9.67E-05	0.04992	1.60E-04
84	9.51E-12	0.16467	8.20E-05	0.02041	7.39E-04
85	3.03E-12	0.1641	6.96E-05	0.10632	3.07E-04
86	7.19E-12	0.15967	5.83E-05	1.17E-15	5.05E-04
87	9.32E-12	0.15801	4.84E-05	1.60E-15	4.23E-04
88	1.34E-11	0.15702	4.00E-05	1.92E-15	2.62E-04

Table S24 Relaxation fitting parameters for **4S** obtained from CCFIT2.

T / K	χ_S / cm^3 mol^{-1}	χ_T / cm^3 mol^{-1}	τ / s	α	Residual
2	0.02442	7.46328	0.05542	0.29769	0.00927
3	0.02389	5.03338	0.05182	0.28574	0.00536
5	0.01995	3.04253	0.04371	0.2552	0.00572
8	0.01958	1.89571	0.0325	0.21993	0.00535
11	0.01565	1.35996	0.02304	0.18851	0.00424
16	0.0167	0.92409	0.01374	0.14778	0.00305
21	0.01893	0.69346	0.00903	0.11564	0.00178
26	0.0095	0.56274	0.00627	0.12336	0.00222
31	0.01398	0.46682	0.00469	0.10276	9.53E-04
36	0.01915	0.39984	0.00362	0.06857	0.00193
41	0.01361	0.35276	0.00271	0.08702	0.00109
46	0.01656	0.31343	0.00215	0.05279	0.00202
51	0.00892	0.28463	0.00166	0.08648	4.65E-04
56	0.01735	0.25719	0.00134	0.05377	6.29E-04
61	0.00701	0.238	9.72E-04	0.07253	3.12E-04
66	0.01081	0.22153	7.05E-04	0.07627	0.00105
70	0.0062	0.19755	4.33E-04	0.09825	0.01356
73	0.00347	0.19832	3.36E-04	0.06606	8.47E-04
76	0.01929	0.1904	2.64E-04	0.07995	0.0011
78	0.00473	0.18435	2.05E-04	0.11779	0.00191
80	0.04275	0.18029	1.75E-04	0.00183	5.63E-04
81	0.03401	0.16962	1.61E-04	1.36E-14	0.0149
82	0.05455	0.17554	1.45E-04	7.05E-15	7.97E-04
83	0.05577	0.17356	1.35E-04	6.55E-15	0.00156
84	0.02722	0.1725	1.21E-04	9.06E-15	8.62E-04
85	0.06844	0.16957	1.07E-04	7.92E-15	5.71E-04
86	0.07362	0.16807	8.91E-05	1.02E-14	4.99E-04
87	0.07659	0.16485	7.29E-05	1.73E-14	6.96E-04
88	0.06259	0.16521	6.03E-05	2.29E-14	4.63E-04

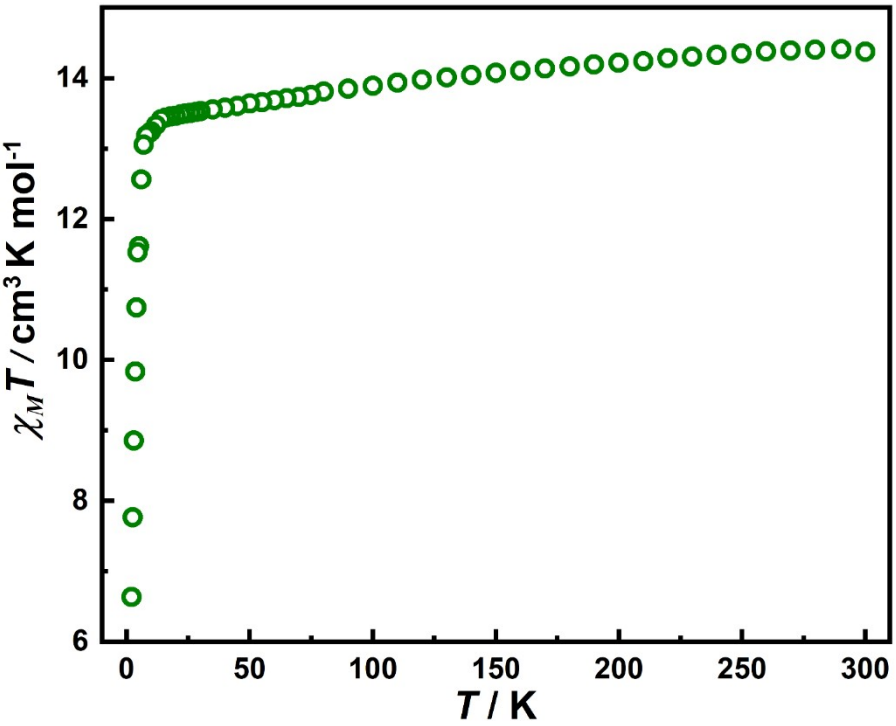

Figure S28. Temperature dependence of the $\chi_M T$ values for **1** performed with a 1000 Oe applied field in the temperature range 2 to 300 K.

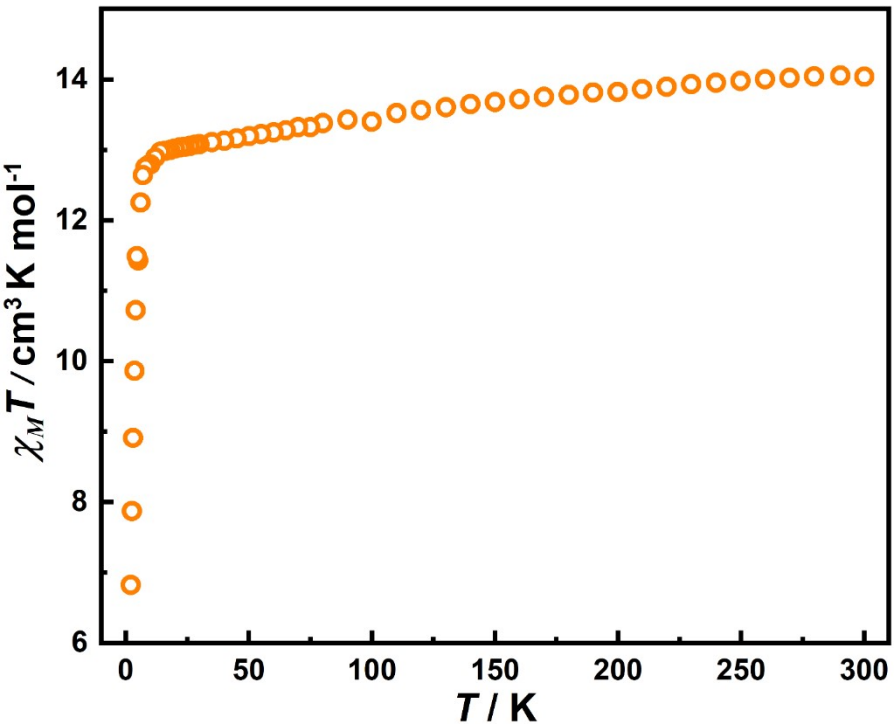

Figure S29. Temperature dependence of the $\chi_M T$ values for **2** performed with a 1000 Oe applied field in the temperature range 2 to 300 K.

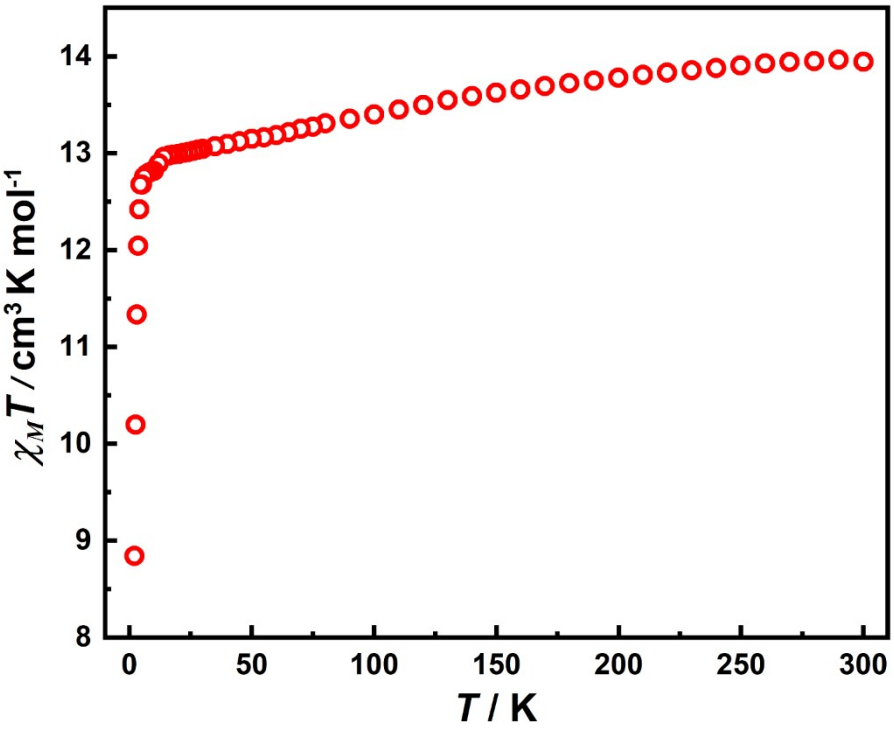

Figure S30. Temperature dependence of the $\chi_M T$ values for **3R** performed with a 1000 Oe applied field in the temperature range 2 to 300 K.

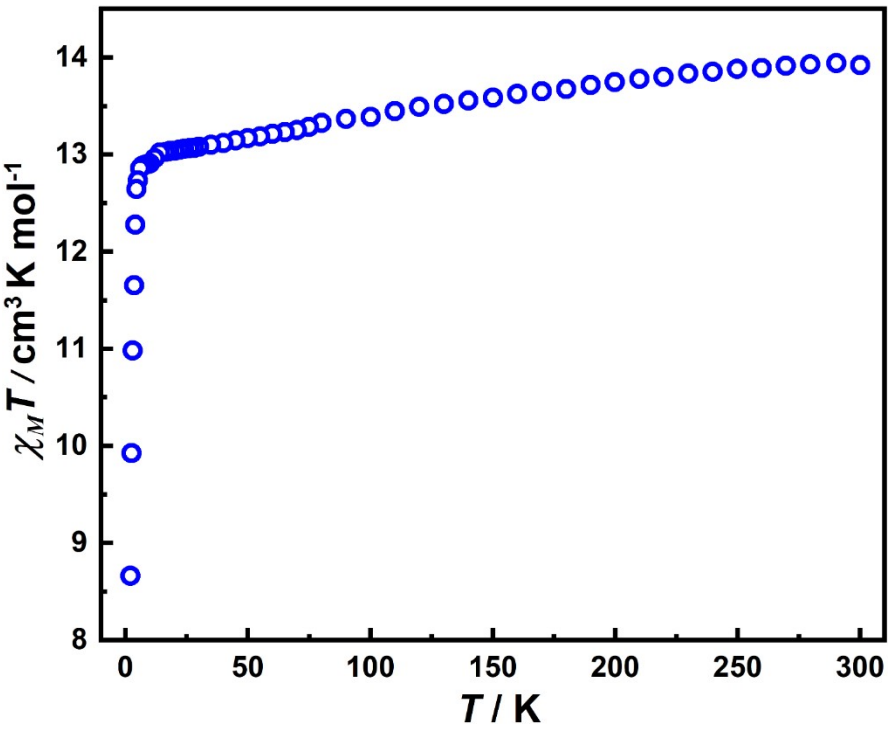

Figure S31. Temperature dependence of the $\chi_M T$ values for **3S** performed with a 1000 Oe applied field in the temperature range 2 to 300 K.

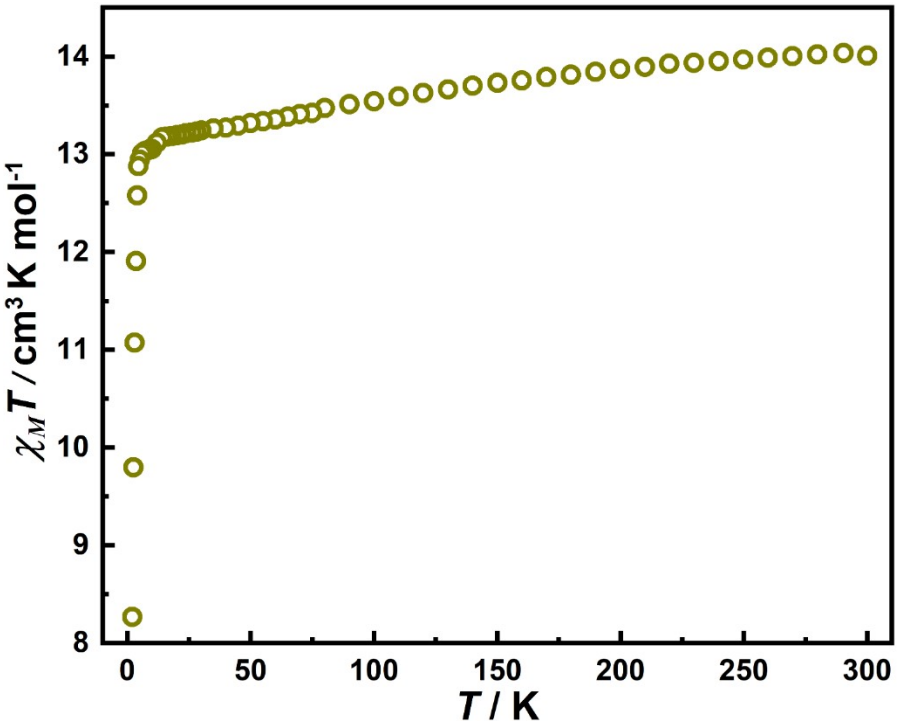

Figure S32. Temperature dependence of the $\chi_M T$ values for **4R** performed with a 1000 Oe applied field in the temperature range 2 to 300 K.

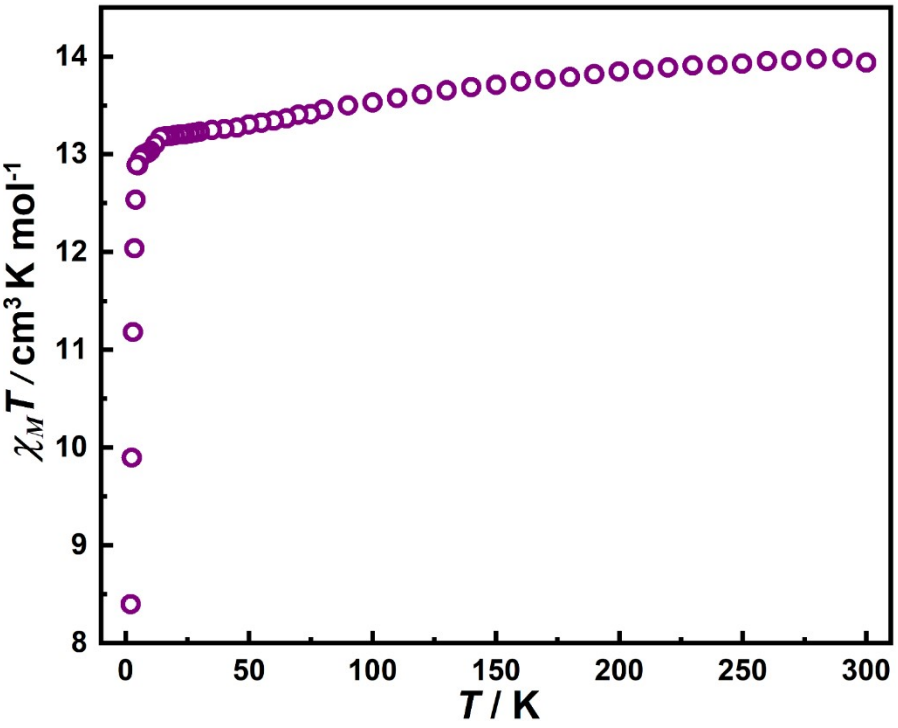

Figure S33. Temperature dependence of the $\chi_M T$ values for **4S** performed with a 1000 Oe applied field in the temperature range 2 to 300 K.

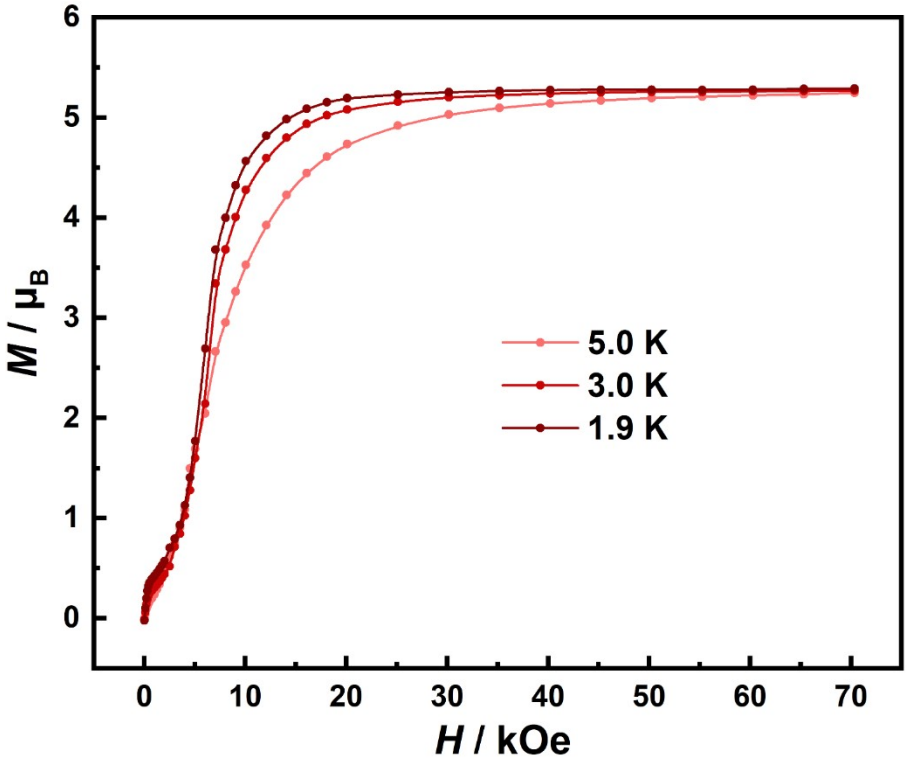

Figure S34. Field dependence of the magnetization at 1.9, 3 and 5 K for **1**.

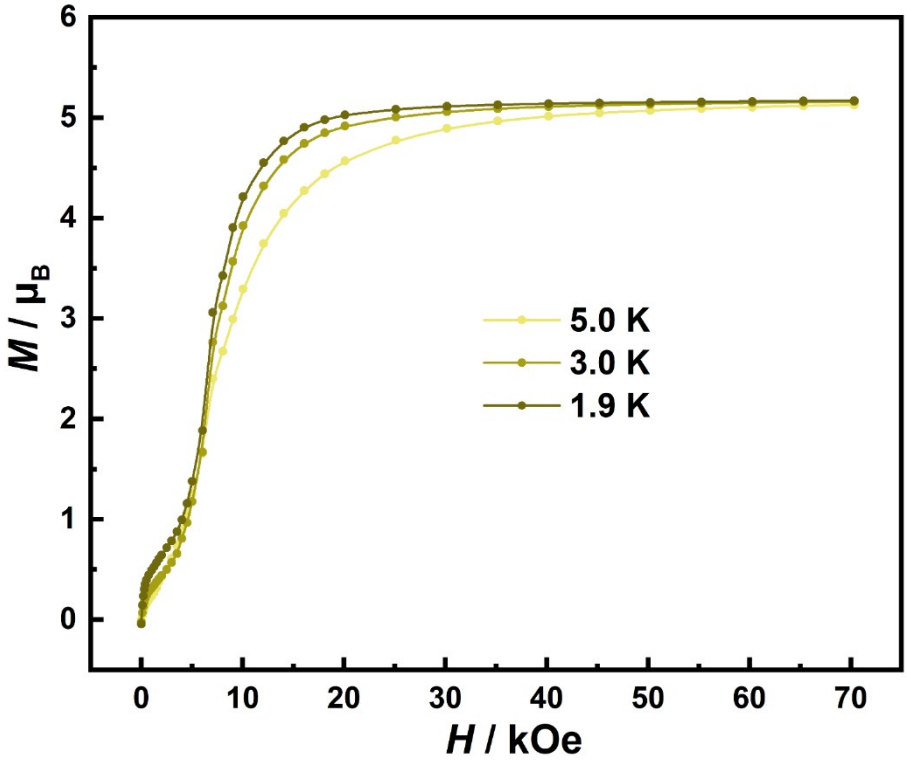

Figure S35. Field dependence of the magnetization at 1.9, 3 and 5 K for **2**.

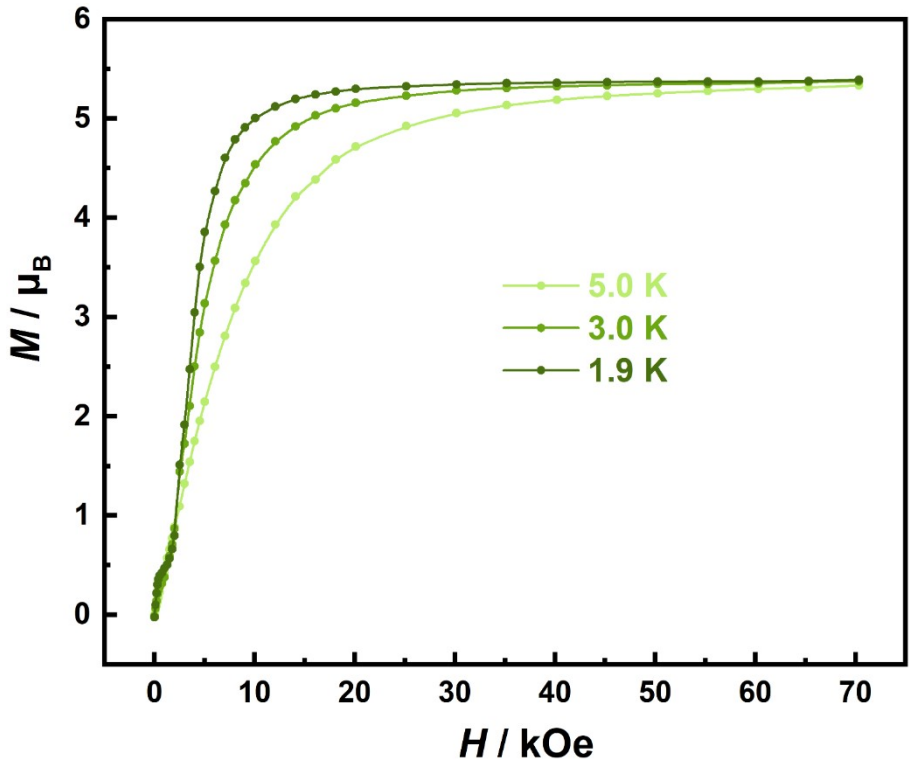

Figure S36. Field dependence of the magnetization at 1.9, 3 and 5 K for **3R**.

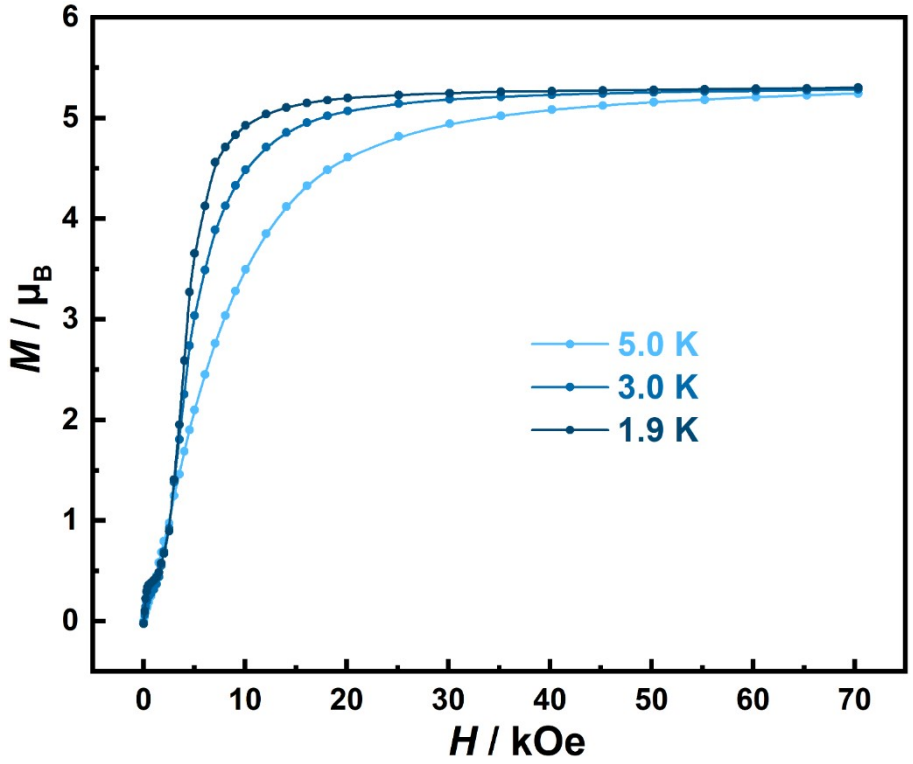

Figure S37. Field dependence of the magnetization at 1.9, 3 and 5 K for **3S**.

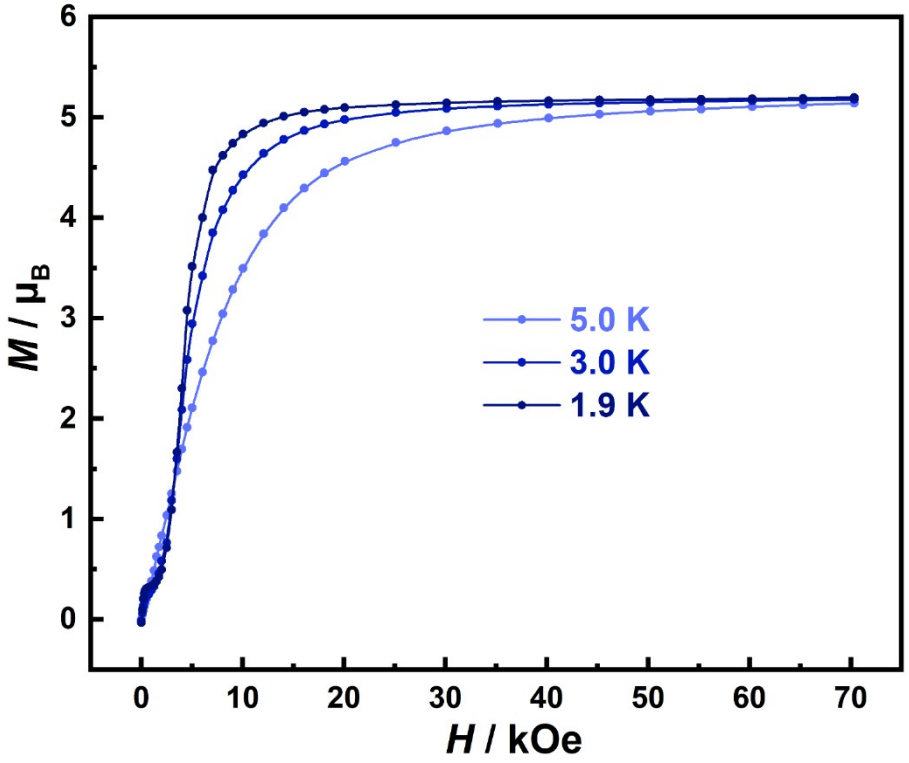

Figure S38. Field dependence of the magnetization at 1.9, 3 and 5 K for **4R**.

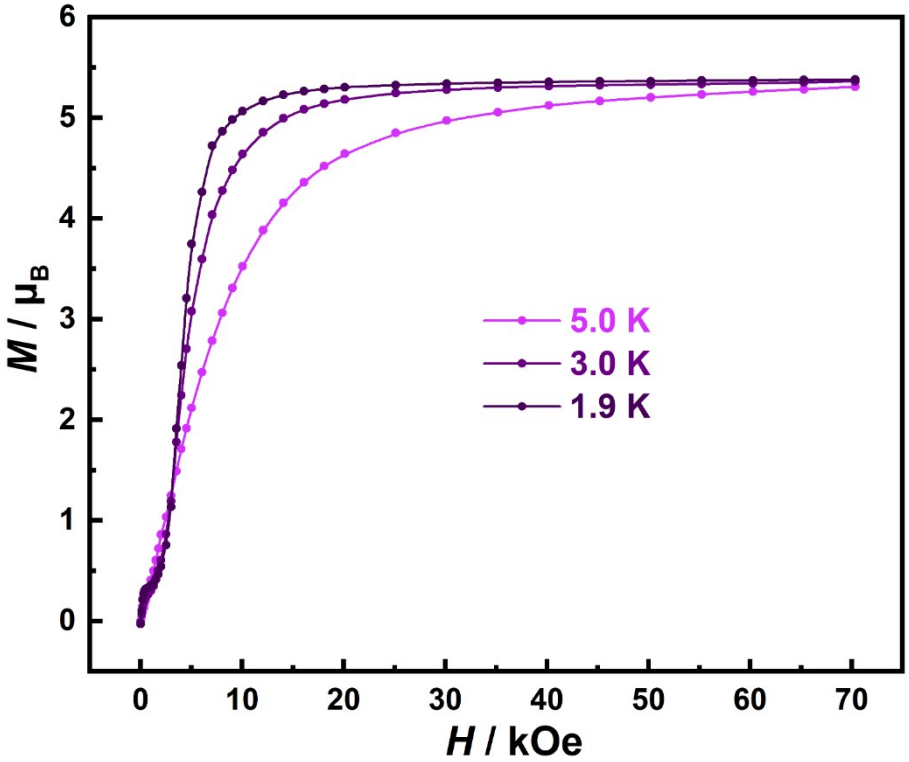

Figure S39. Field dependence of the magnetization at 1.9, 3 and 5 K for **4S**.

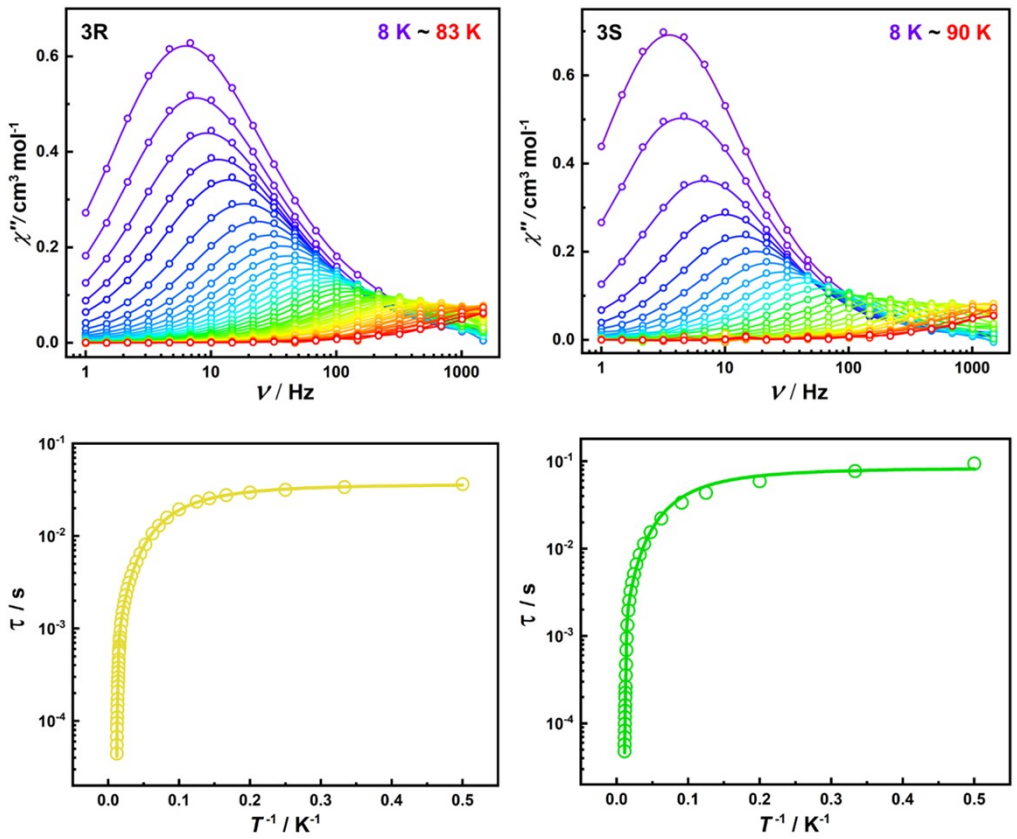

Figure S40. (upper) Frequency dependence of the out-of-phase component of the ac susceptibility for **3R** and **3S** at the temperatures shown. (bottom) Temperature dependence of the magnetic relaxation times plotted as τ versus T^{-1}. Solid lines are fits using the parameters in Table 1. Data were collected in an ac field of 3 Oe and zero dc field.

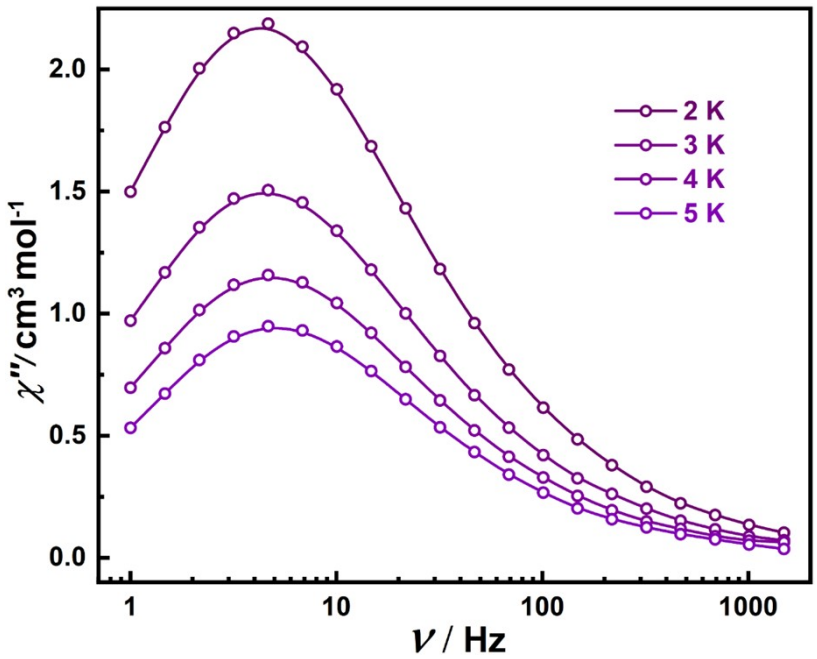

Figure S41. Frequency dependence of the out-of-phase susceptibility for **3R** in zero dc field at ν = 1-1488 Hz and temperatures of 2-5 K.

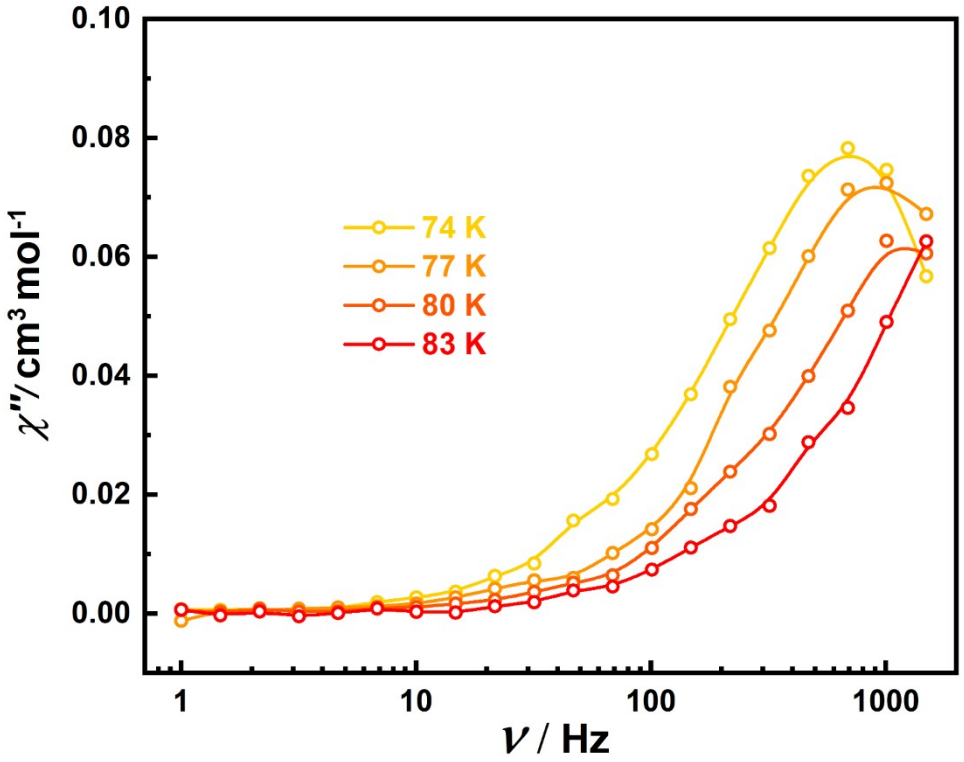

Figure S42. Frequency dependence of the out-of-phase susceptibility for **3R** in zero dc field at ν = 1-1488 Hz and temperatures of 74-83 K.

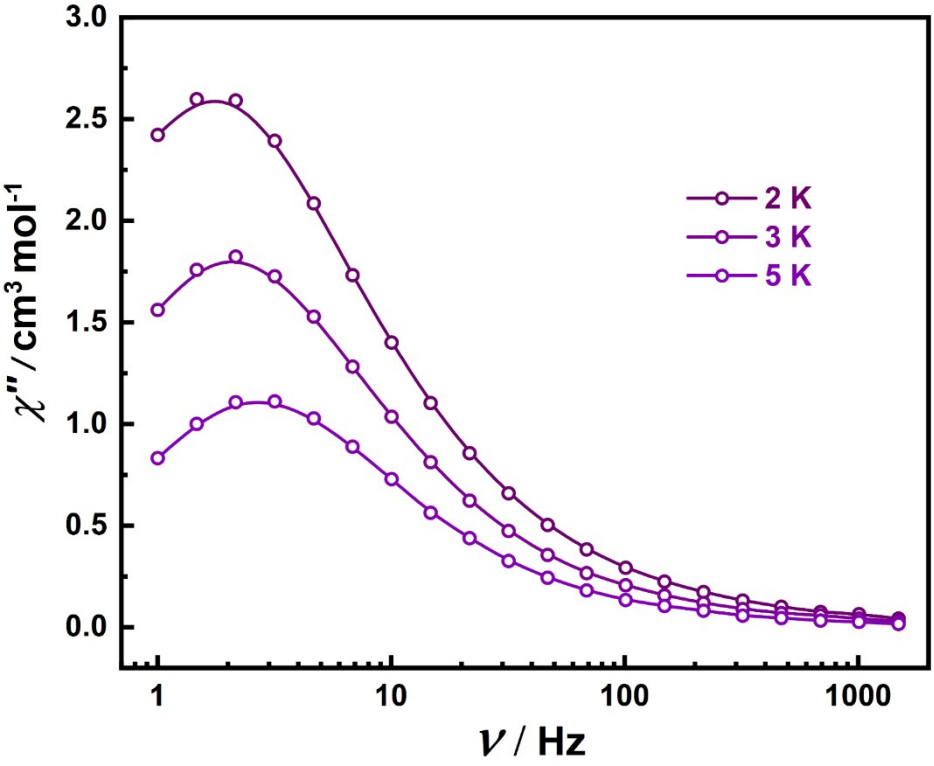

Figure S43. Frequency dependence of the out-of-phase susceptibility for **3S** in zero dc field at ν = 1-1488 Hz and temperatures of 2-5 K.

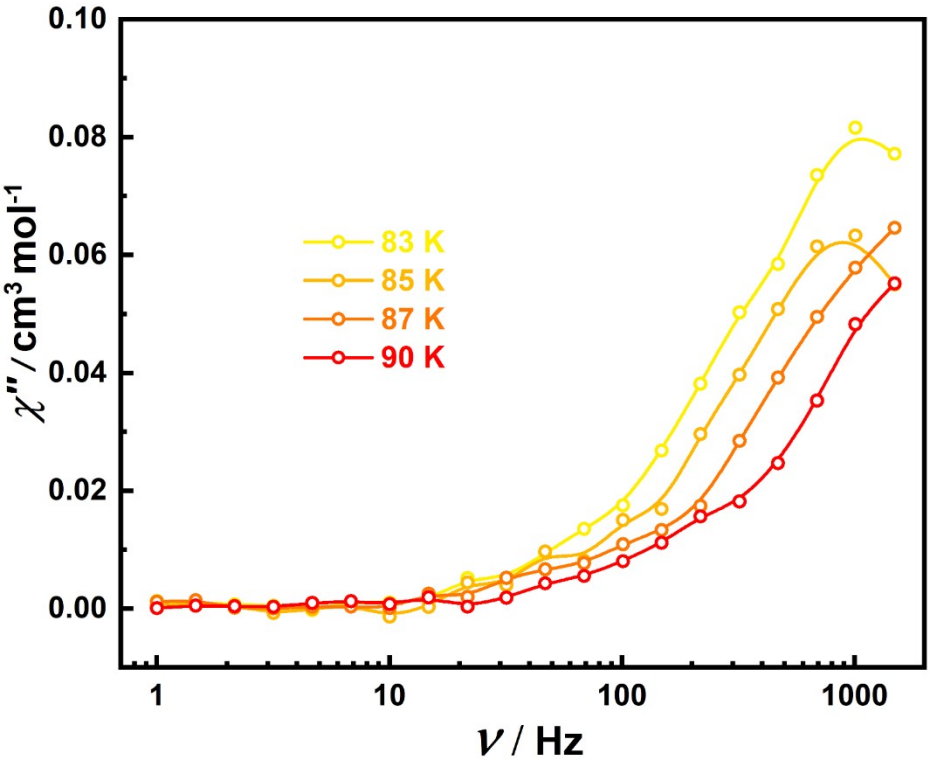

Figure S44. Frequency dependence of the out-of-phase susceptibility for **3S** in zero dc field at ν = 1-1488 Hz and temperatures of 83-90 K.

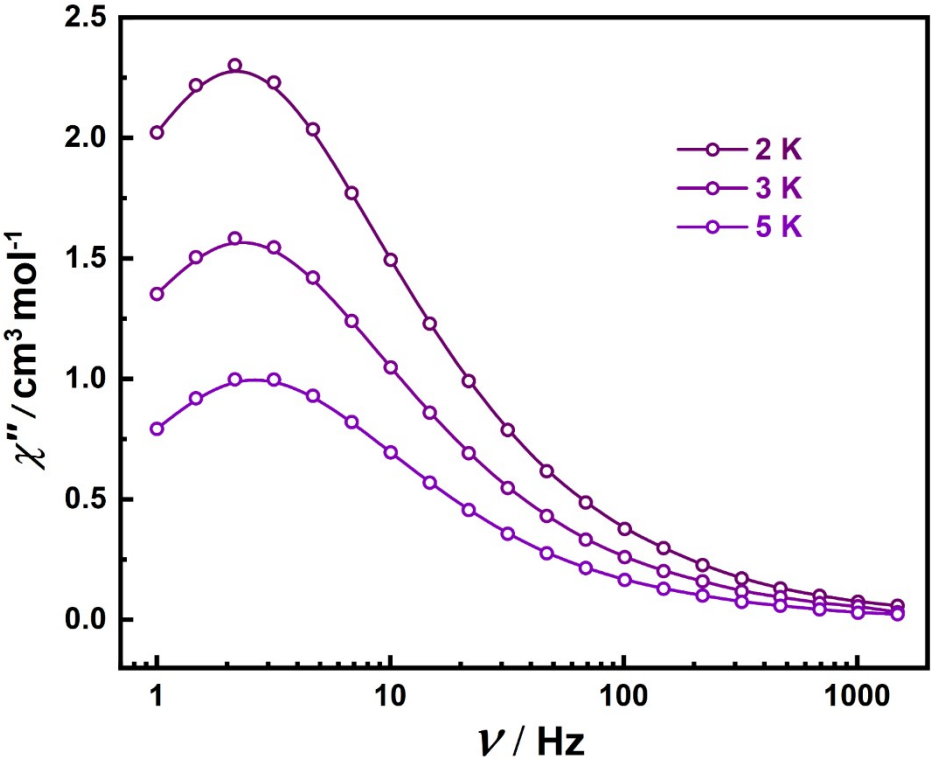

Figure S45. Frequency dependence of the out-of-phase susceptibility for **4R** in zero dc field at ν = 1-1488 Hz and temperatures of 2-5 K.

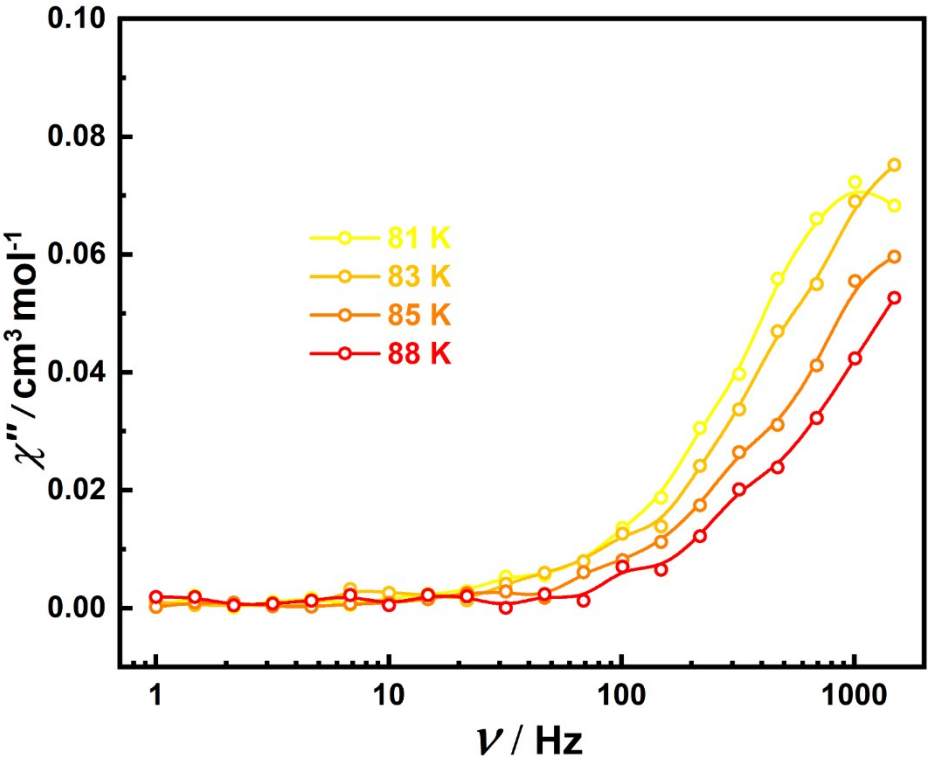

Figure S46. Frequency dependence of the out-of-phase susceptibility for **4R** in zero dc field at ν = 1-1488 Hz and temperatures of 81-88 K.

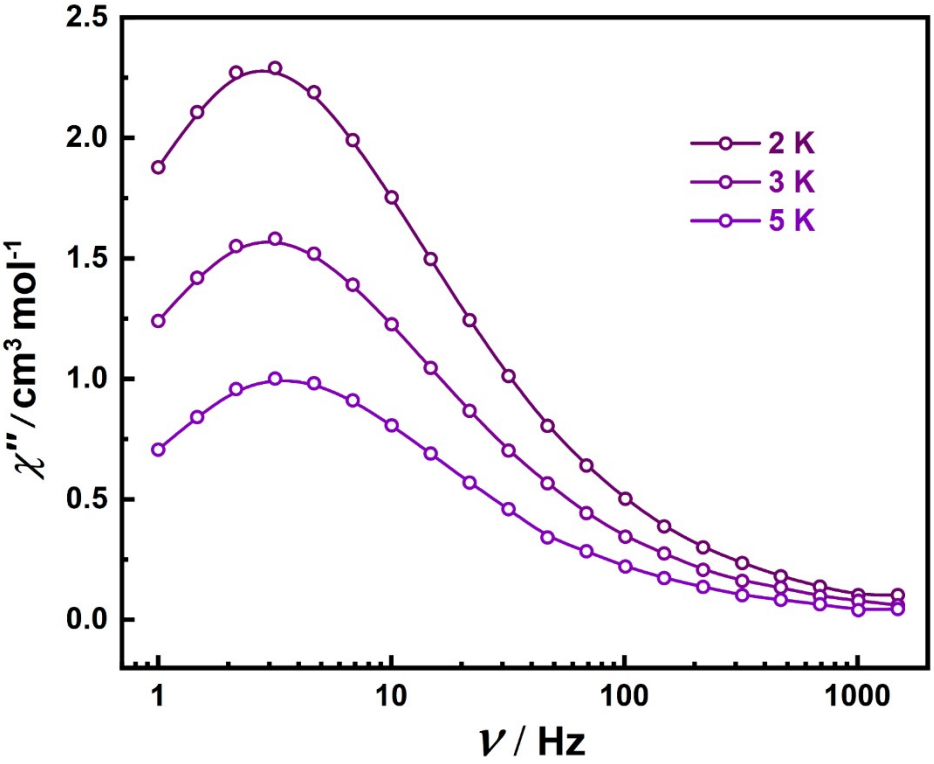

Figure S47. Frequency dependence of the out-of-phase susceptibility for **4S** in zero dc field at ν = 1-1488 Hz and temperatures of 2-5 K.

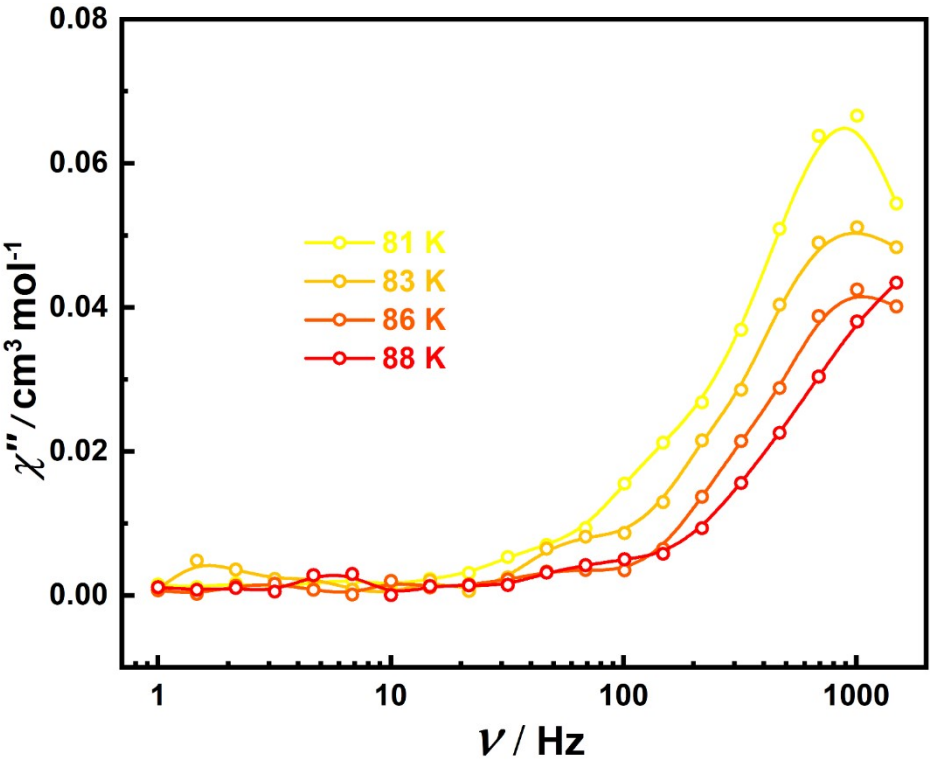

Figure S48. Frequency dependence of the out-of-phase susceptibility for **4S** in zero dc field at ν = 1-1488 Hz and temperatures of 81-88 K.

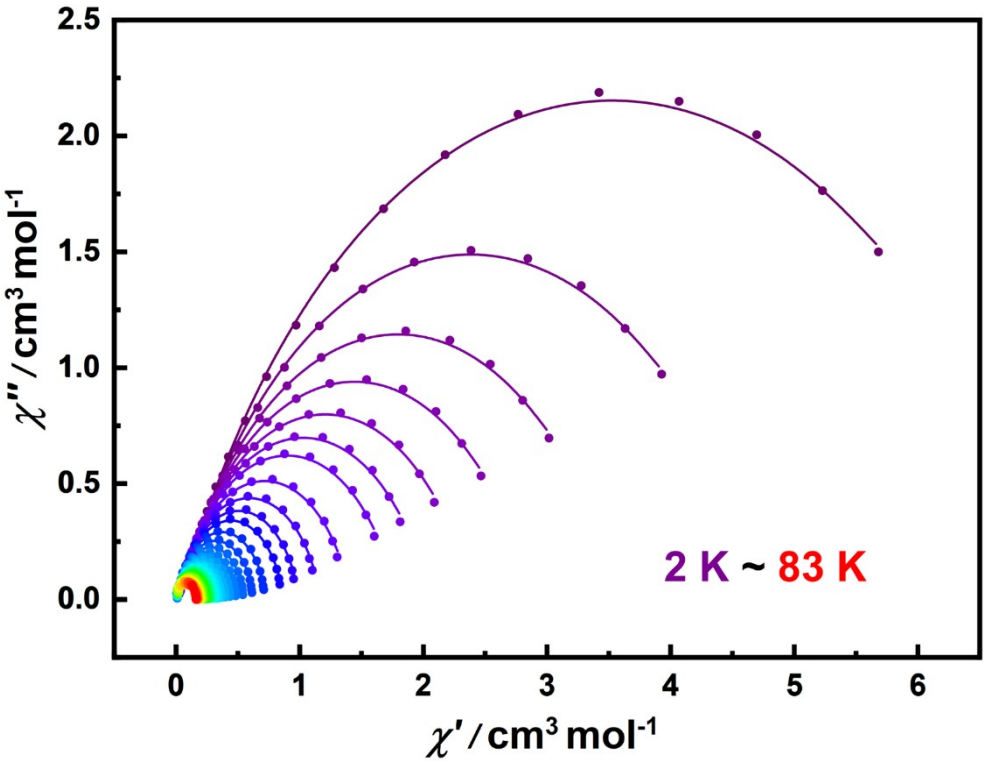

Figure S49. Cole-Cole plots for the AC susceptibilities in zero dc field for **3R** from 2-83 K. Solid lines represent fits to the data using a modified Debye model.

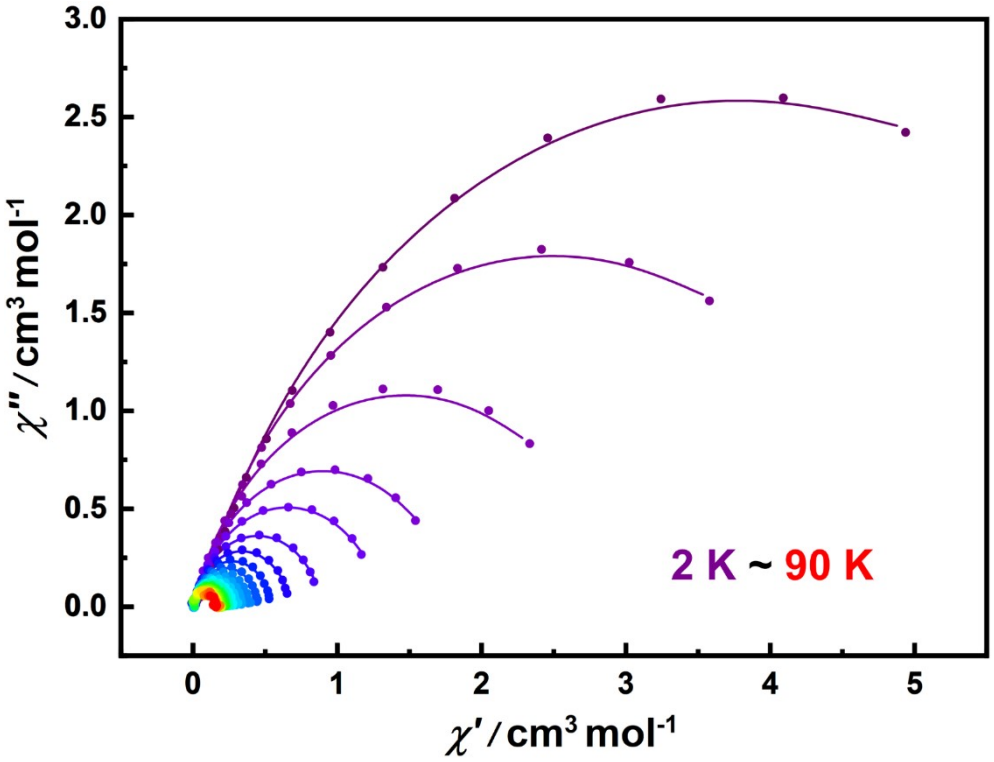

Figure S50. Cole-Cole plots for the AC susceptibilities in zero dc field for **3S** from 2-90 K. Solid lines represent fits to the data using a modified Debye model.

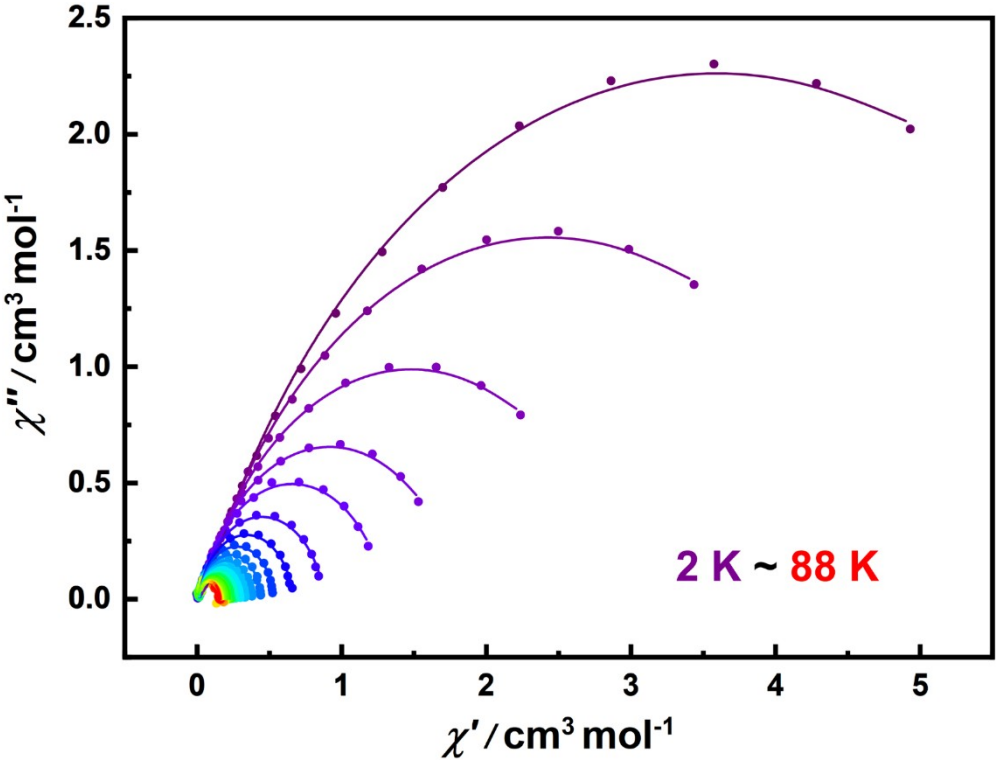

Figure S51. Cole-Cole plots for the AC susceptibilities in zero dc field for **4R** from 2-88 K. Solid lines represent fits to the data using a modified Debye model.

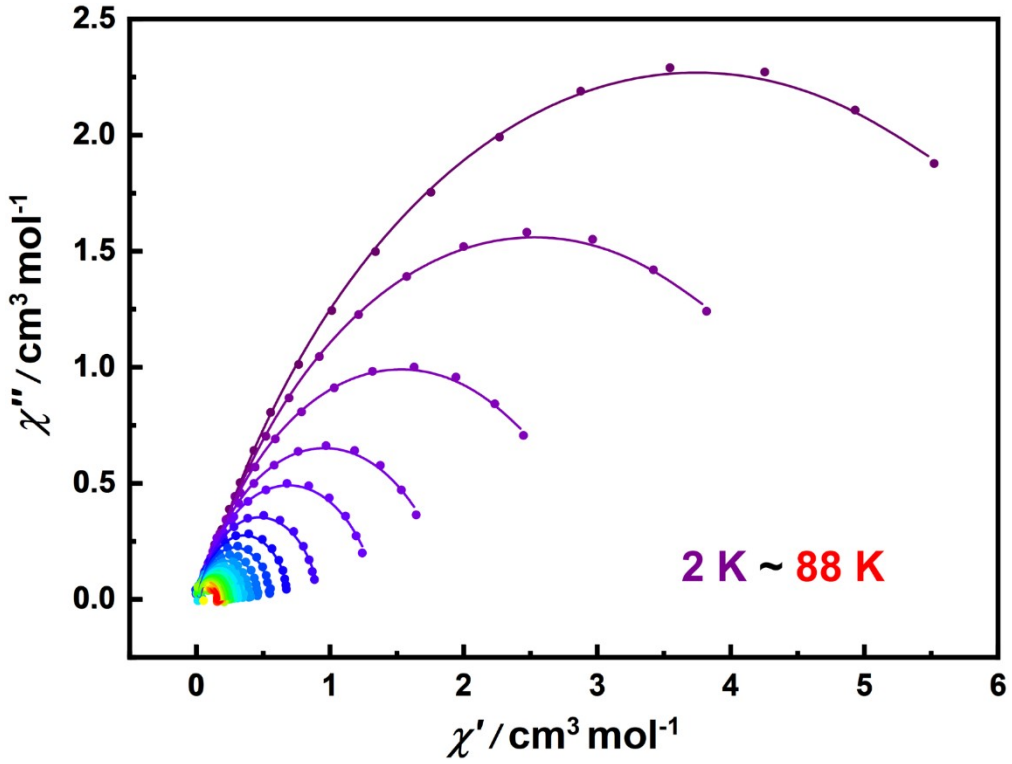

Figure S52. Cole-Cole plots for the AC susceptibilities in zero dc field for **4S** from 2-88 K. Solid lines represent fits to the data using a modified Debye model.

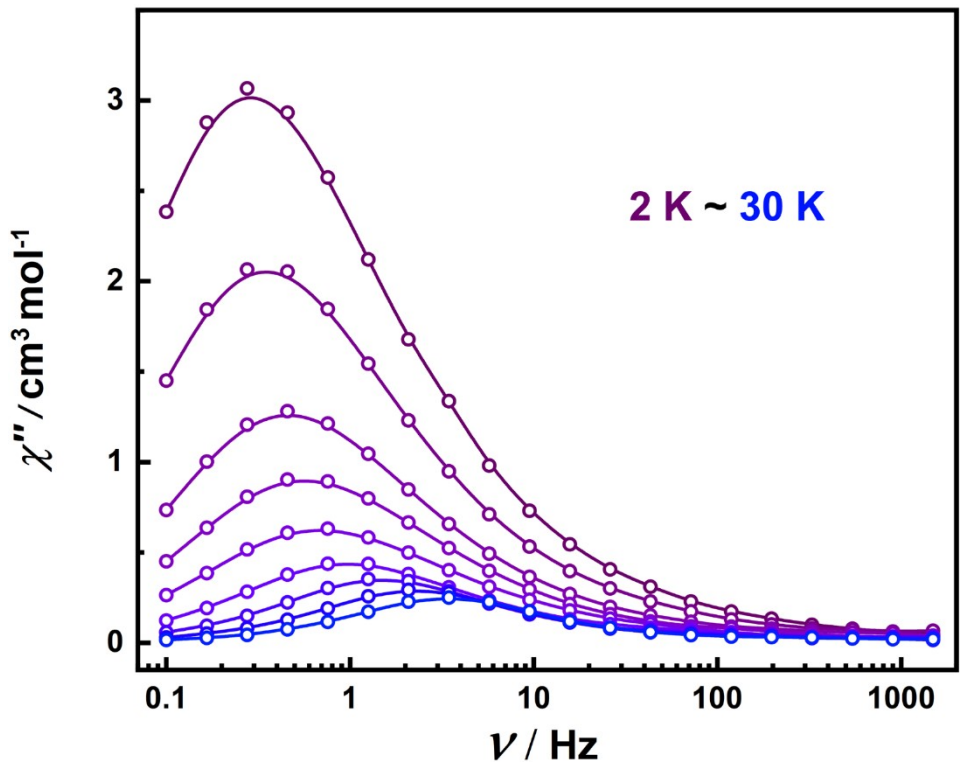

Figure S53. Frequency dependence of the out-of-phase susceptibility for **1** in zero dc field at ν = 0.1-1488 Hz and temperatures of 2-30 K.

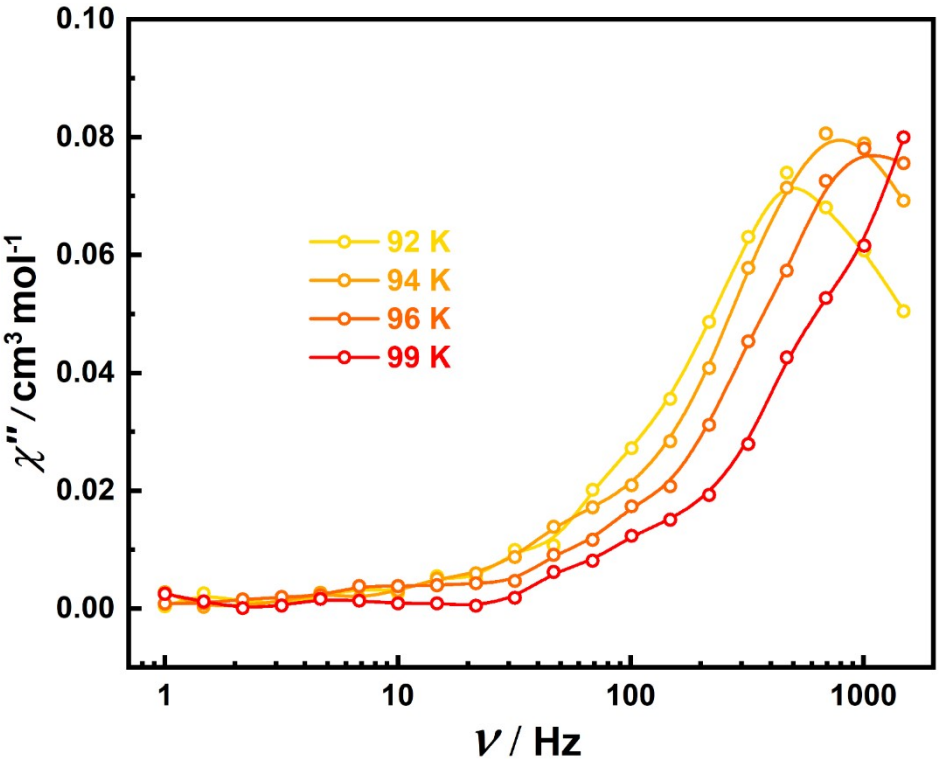

Figure S54. Frequency dependence of the out-of-phase susceptibility for **1** in zero dc field at ν = 1-1488 Hz and temperatures of 92-99 K.

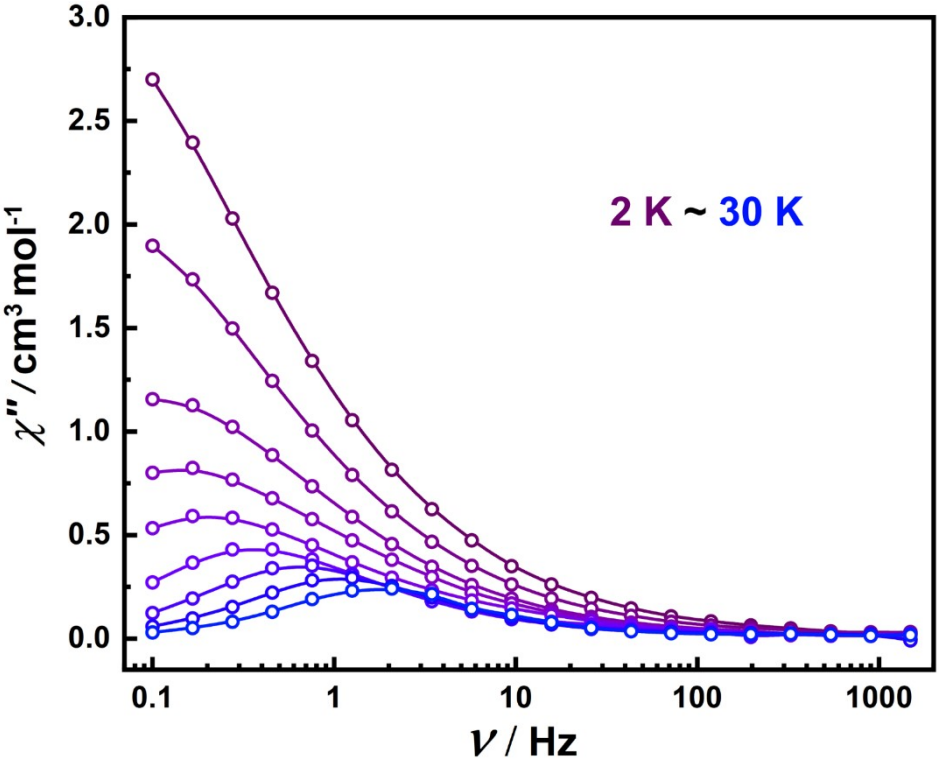

Figure S55. Frequency dependence of the out-of-phase susceptibility for **2** in zero dc field at ν = 0.1-1488 Hz and temperatures of 2-30 K.

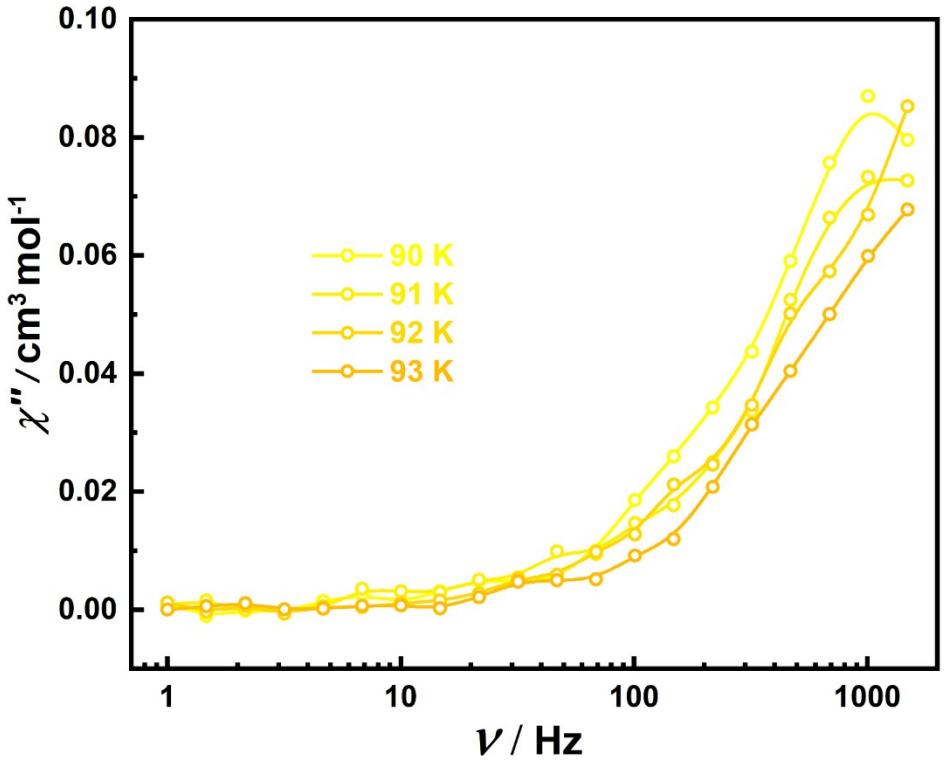

Figure S56. Frequency dependence of the out-of-phase susceptibility for **2** in zero dc field at ν = 1-1488 Hz and temperatures of 90-93 K.

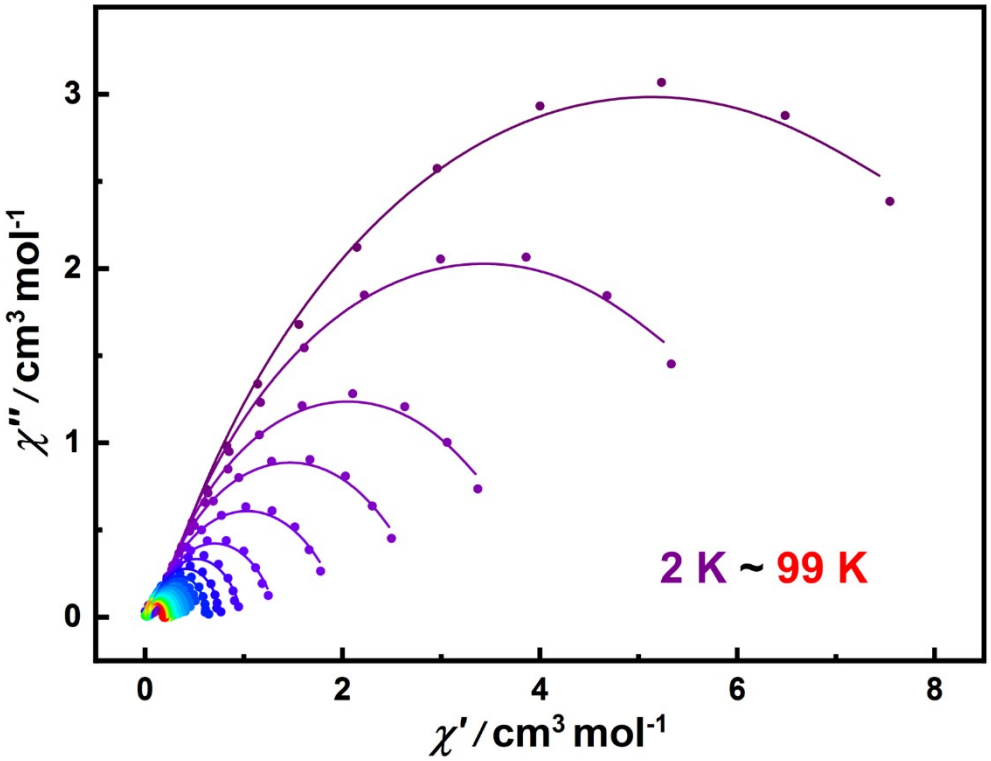

Figure S57. Cole-Cole plots for the AC susceptibilities in zero dc field for **1** from 2-99 K. Solid lines represent fits to the data using a modified Debye model.

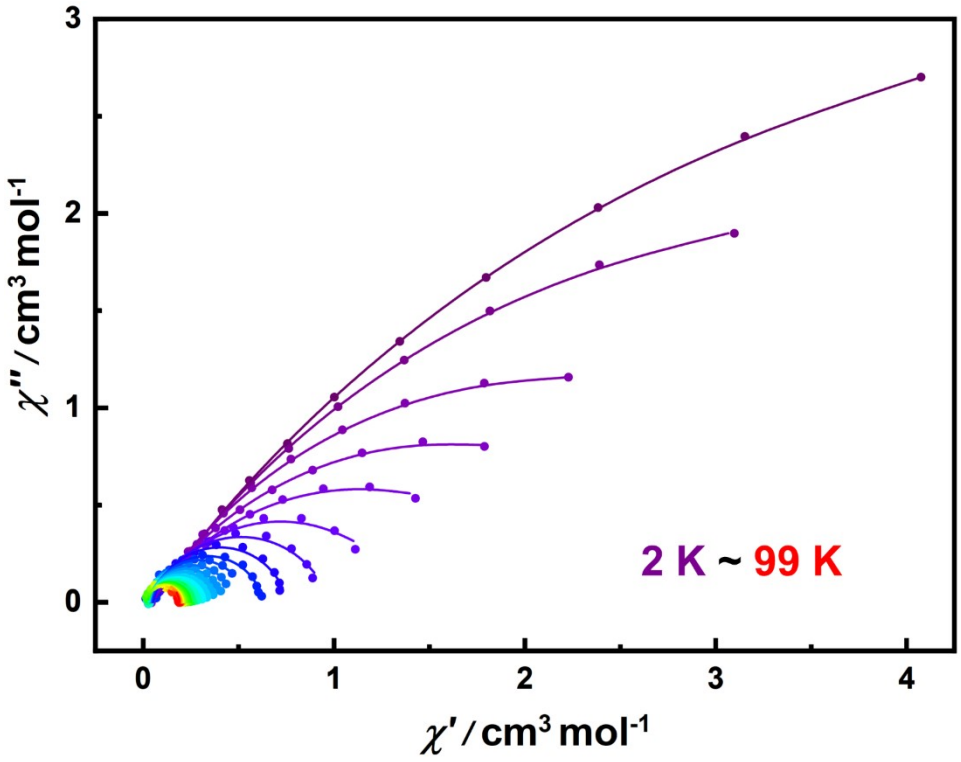

Figure S58. Cole-Cole plots for the AC susceptibilities in zero dc field for **2** from 2-99 K. Solid lines represent fits to the data using a modified Debye model.

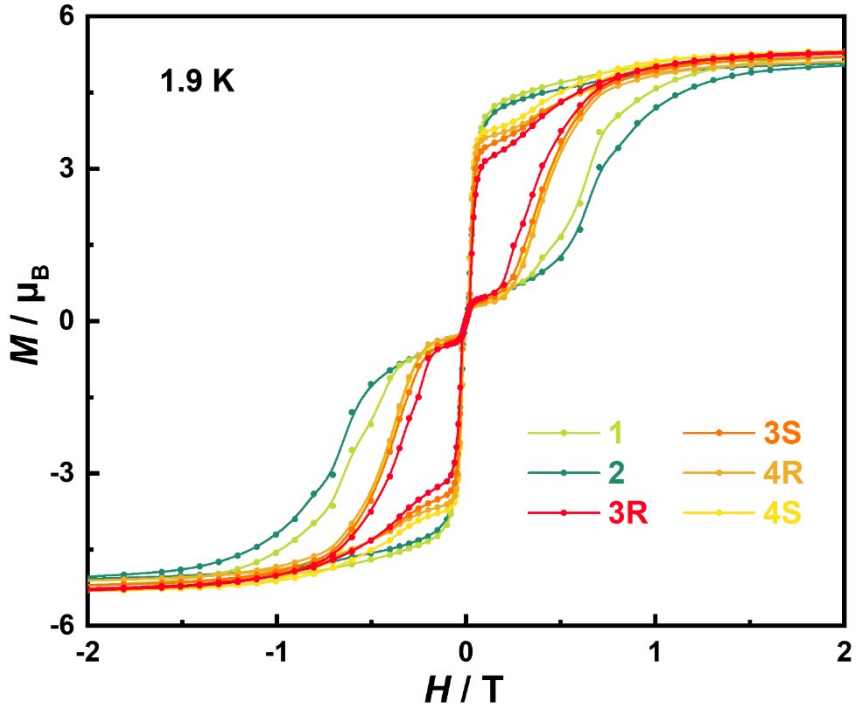

Figure S59. Magnetic hysteresis measurements of **1**, **2**, **3R**, **3S**, **4R** and **4S** at 1.9 K with an average sweep rate of 4 mT s^{-1}.

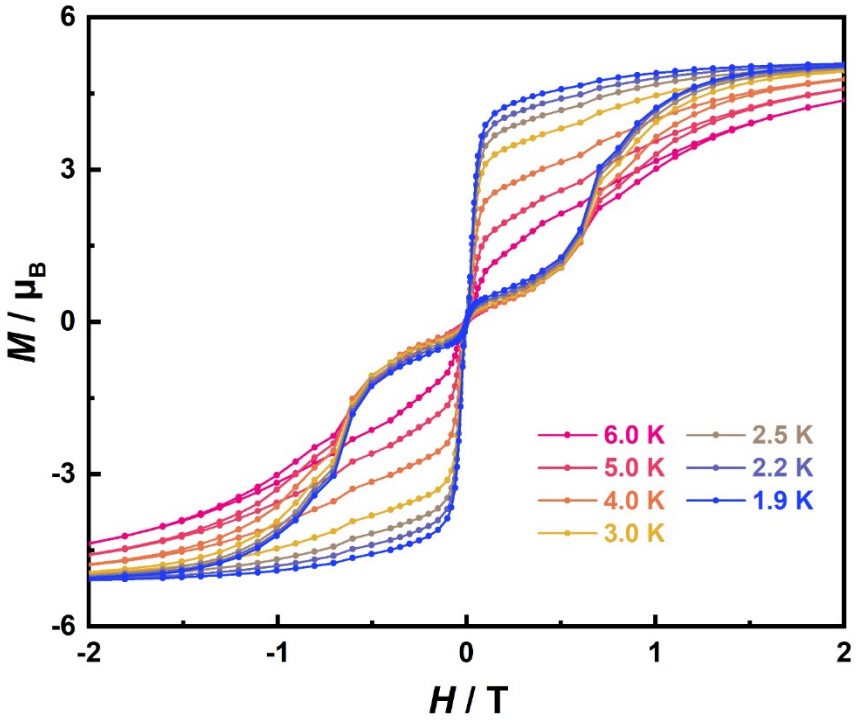

Figure. S60 Magnetic hysteresis measurements for **2** collected at 1.9-6.0 K with an average sweep rate of 4 mT s^{-1}.

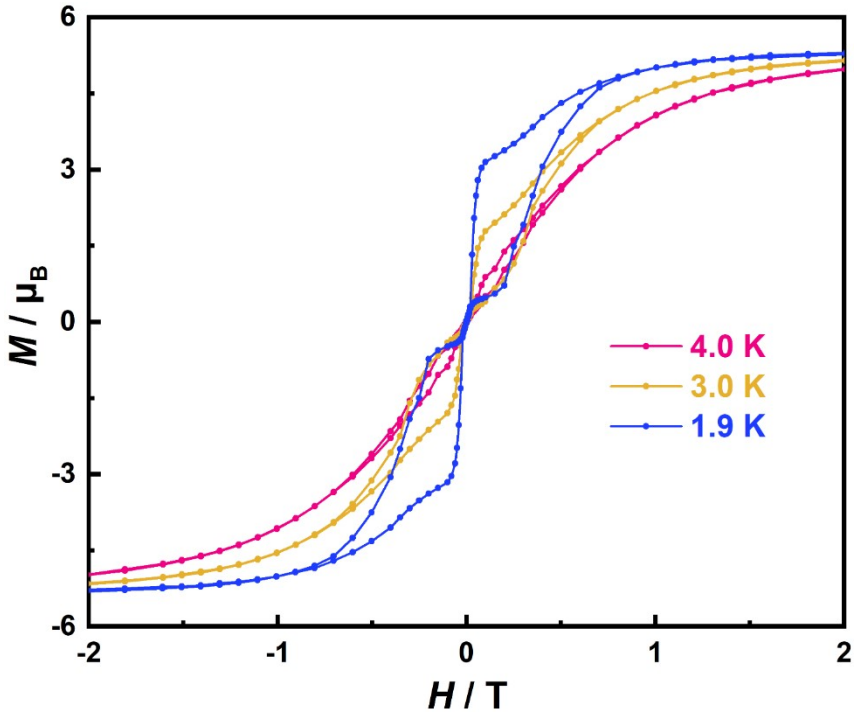

Figure S61. Magnetic hysteresis measurements of **3R** collected at 1.9-4.0 Kwith an average sweep rate of 4 mT s^{-1}.

V. Computational details

Electronic structure calculations were performed using the ORCA 5.0.3 package.[10] The Cartesian coordinates for the input file were taken from the X-Ray structure (excluding the counter ions and solvent molecules). Dysprosium was described by the SARC2-QZVP basis set[11] and other elements were described by Def2-TZVP basis.[12] Scalar relativistic effects were included by the DKH2 Hamiltonian.[13-15] CASSCF(9,7)[16] calculations include the seven 4f orbitals of the Dy^{III} ion in the active space, with 21, 224, and 490 sextet, quartet, and doublet roots, respectively. For lanthanides SMM calculations is necessary to represent the spin–orbit coupling operator in a basis of multideterminant wave functions. Thus, after convergence of CASSCF energies, spin−orbit coupling (SOC) effects were included in a subsequent quasi-degenerate perturbation theory (QDPT) step. Tunnelling relaxation times were calculated according to a model based on intermolecular spin dipolar interactions.[17] Input data for this methodology are the crystallographic information file (CIF) and CASSCF(9,7)/QDPT energies and g-tensors for the eight Kramers' doublets associated with ground Dy^{III} multiplet. This user-friendly routine can be obtained free of charge upon request to the author.

Table S25. CASSCF calculated electronic states for **1** and **2**.

	1		**2**	
KDs	**E/cm^{-1}**	***g*-tensors**	**E/cm^{-1}**	***g*-tensors**
1	0	0.000102 0.000112 19.489022	0	0.000103 0.000110 19.489438
2	537.72	0.050364 0.050860 16.684097	542.16	0.051186 0.051735 16.681850
3	949.86	0.014953 0.052618 13.831254	957.68	0.027697 0.045236 13.819505
4	1192.57	0.625511 0.958586 9.218578	1201.45	0.660707 1.135751 8.995357
5	1267.07	0.651953 3.771521 12.666283	1274.94	0.625469 2.827451 12.617979
6	1277.93	1.004379 3.690449 10.663599	1285.84	1.236696 4.800832 10.007486
7	1319.07	0.744137 1.841056 5.111886	1324.95	0.881880 1.595879 5.416910
8	1376.58	0.774722 8.412806 10.806926	1383.92	0.792336 7.863529 11.258874

Table S26. CASSCF calculated electronic states for **3S** and **3R**.

	3S		**3R**	
KDs	**E/cm^{-1}**	***g*-tensors**	**E/cm^{-1}**	***g*-tensors**
1	0	0.000464 0.000489 19.484369	0	0.000388 0.000414 19.485246
2	512.61	0.069717 0.073767 16.678489	514.45	0.065934 0.069288 16.680730
3	896.35	0.016608 0.160763 13.679481	901.33	0.037220 0.116477 13.711378
4	1099.06	2.712399 5.339346 7.414779	1110.33	2.741347 5.003177 6.711784
5	1144.06	2.260863 5.199314 10.268710	1155.05	1.741232 5.597080 11.243914
6	1179.11	0.628987 3.575400 9.804774	1188.20	0.834310 3.214612 9.715628
7	1218.19	0.013138 0.627633 12.450421	1228.18	0.254759 0.572770 12.119114
8	1285.22	1.282220 4.349747 14.413910	1292.21	1.292509 4.986754 13.830846

Table S27. CASSCF calculated electronic states for **4S** and **4R**.

	4S		**4R**	
KDs	**E/cm^{-1}**	***g*-tensors**	**E/cm^{-1}**	***g*-tensors**
1	0	0.000445 0.000474 19.484833	0	0.000432 0.000462 19.484533
2	508.34	0.068325 0.072361 16.681829	508.36	0.069857 0.073793 16.680953
3	889.88	0.037327 0.130218 13.692556	889.44	0.049876 0.119514 13.687534
4	1093.06	3.098708 5.289418 6.460718	1092.59	3.012777 4.926132 6.339888
5	1134.47	1.746710 5.566728 11.271112	1134.19	1.697208 5.678658 11.274236
6	1173.20	0.885268 2.669129 9.707984	1170.65	0.759181 2.490877 9.939726
7	1214.27	0.176498 0.754191 13.374452	1212.42	0.300440 0.655248 12.872376
8	1276.81	1.286675 4.691610 14.029073	1275.84	1.300516 4.721200 14.012573

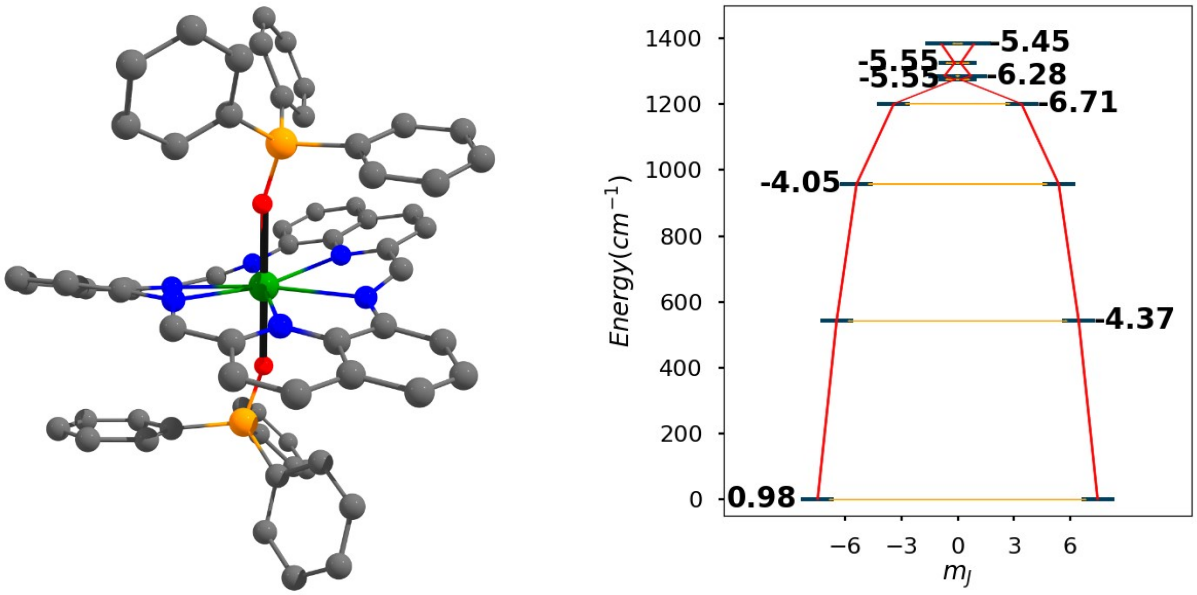

Figure S62. (Left) Calculated orientation of the main magnetic axis of the ground Kramers doublet and (Right) Ab initio double well potential for **2**. The blue bars indicate the Kramers doublets. Tunnelling relaxation times (τ_{QTM}) between the connecting pairs are indicated as orange lines and the values are represented on a logarithmic scale.

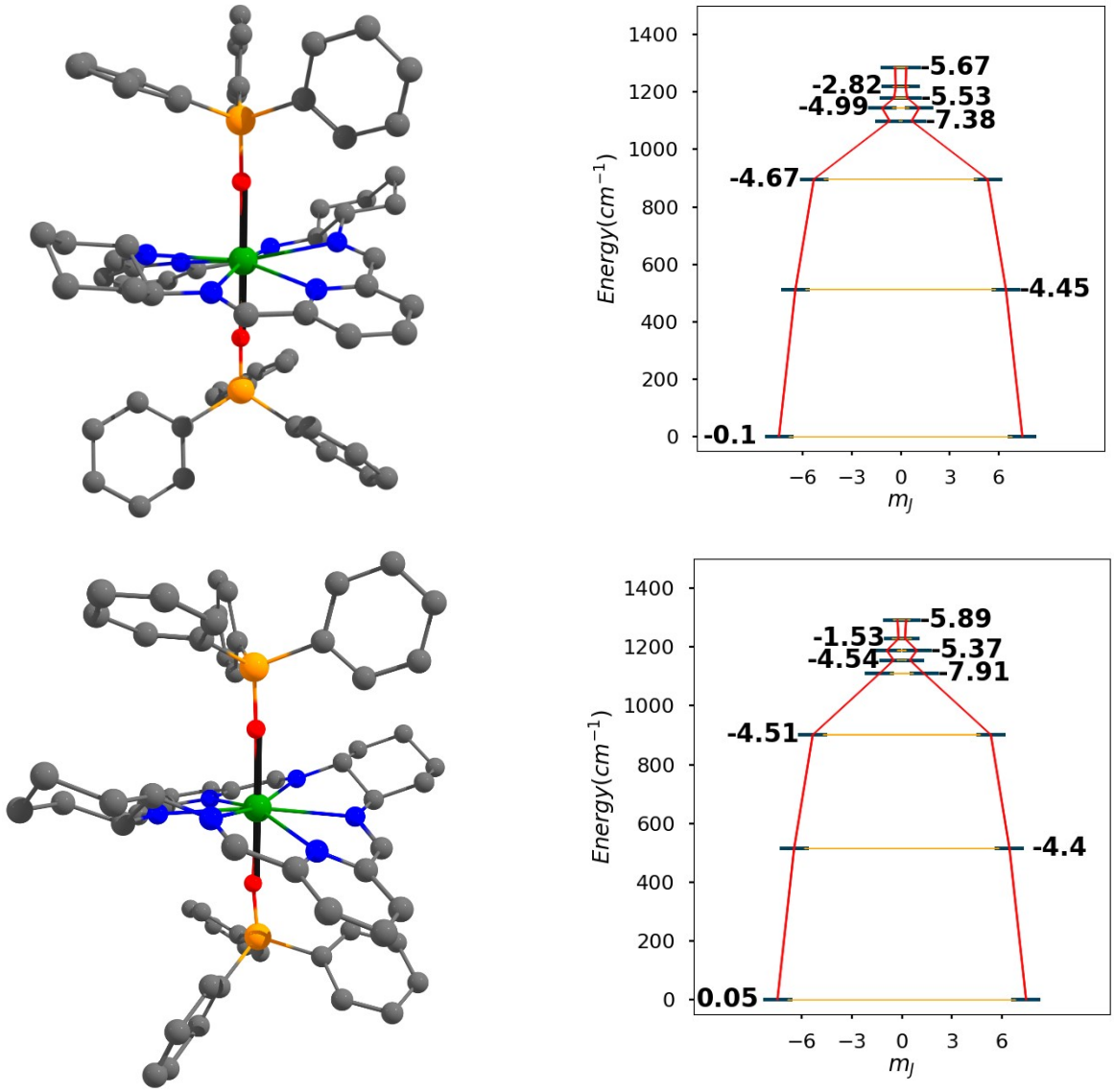

Figure S63. Calculated orientation of the main magnetic axis of the ground Kramers doublet and (Right) Ab initio double well potential for **3S** (up) and **3R** (bottom). The blue bars indicate the Kramers doublets. Tunnelling relaxation times (τ_{QTM}) between the connecting pairs are indicated as orange lines and the values are represented on a logarithmic scale.

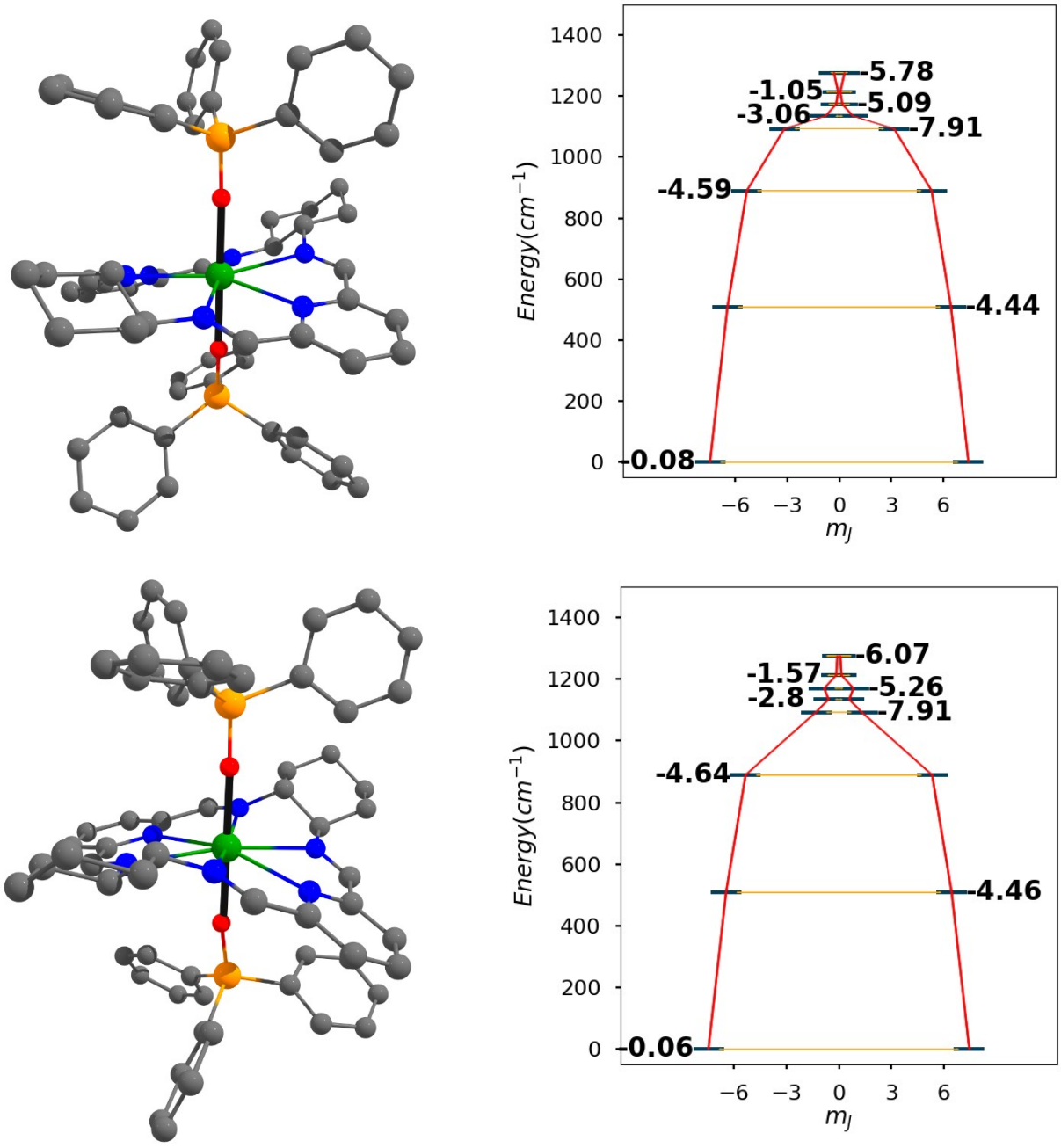

Figure S64. (Left) Calculated orientation of the main magnetic axis of the ground Kramers doublet and (Right) Ab initio double well potential for **4S** (up) and **4R** (bottom). The blue bars indicate the Kramers doublets. Tunnelling relaxation times (τ_{QTM}) between the connecting pairs are indicated as orange lines and the values are represented on a logarithmic scale.

VI. References

1. G. M. Sheldrick, *Acta Cryst. A*, 2015, **71**, 3-8.
2. G. M. Sheldrick, *Acta Cryst. A*, 2008, **64**, 112-122.
3. O. V. Dolomanov, L. J. Bourhis, R. J. Gildea, J. A. K. Howard and H. Puschmann, *J. Appl. Crystallogr.*, 2009, **42**, 339-341.
4. G. A. Bain and J. F. Berry, *J. Chem. Educ.*, 2008, **85**, 532.
5. G. Xue, J. S. Bradshaw, N. K. Dalley, P. B. Savage, K. E. Krakowiak, R. M. Izatt, L. Prodi, M. Montalti and N. Zaccheroni, *Tetrahedron*, 2001, **57**, 7623-7628.
6. J. L. Greenfield, F. J. Rizzuto, I. Goldberga and J. R. Nitschke, *Angew. Chem. Int. Ed.*, 2017, **56**, 7541-7545.
7. A. Music, A. N. Baumann, P. Spieß, A. Plantefol, T. C. Jagau and D. Didier, *J. Am. Chem. Soc.*, 2020, **142**, 4341-4348.
8. M. Pinsky and D. Avnir, *Inorg. Chem.*, 1998, **37**, 5575-5582.
9. D. Casanova, J. Cirera, M. Llunell, P. Alemany, D. Avnir and S. Alvarez, *J. Am. Chem. Soc.*, 2004, **126**, 1755-1763.
10. F. Neese, *WIREs Comput Mol Sci.*, 2022, **12**, e1606.
11. D. Aravena, F. Neese and D. A. Pantazis, *J. Chem. Theory Comput.*, 2016, **12**, 1148-1156.
12. F. Weigend and R. Ahlrichs, *Phys. Chem. Chem. Phys.*, 2005, **7**, 3297-3305.
13. N. Rösch, S. Krüger, M. Mayer and V. A. Nasluzov, in *Theoretical and Computational Chemistry*, ed. J. M. Seminario, Elsevier, 1996, vol. 4, pp. 497-566.
14. T. Nakajima and K. Hirao, *Chem. Rev.*, 2012, **112**, 385-402.
15. M. Reiher, *WIREs Comput Mol Sci.*, 2012, **2**, 139-149.
16. P.-Å. Malmqvist and B. O. Roos, *Chem. Phys. Lett.*, 1989, **155**, 189-194.
17. D. Aravena, *J. Phys. Chem. Lett.*, 2018, **9**, 5327-5333.